Disease exacerbation in MYOrganoids derived from Duchenne Muscular Dystrophy iPSC reveals limitations of microdystrophin therapeutic efficacy

Laura Palmieri [1,2], Louna Pili[1,2] , Abbass Jaber, [1,2] Ai Vu Hong [1,2] , Melissa Moula[1,2], Riyad El-Khoury [1,2,3], Guy Brochiet [3 ,4], Anne Bigot [5], David Israeli [1,2], Isabelle Richard [1,2], Sonia Albini [1,2*]

[1]Genethon, 91100 Evry, France; [2]Université Paris-Saclay, Univ Evry, Inserm, Généthon, Integrare research unit UMR_S951, 91000, Evry, France. [3]Institut de Myologie, Neuromuscular Morphology Unit, Groupe Hospitalier Pitié-Salpêtrière, Paris, France.[4]AP-HP, Centre de Référence de Pathologie Neuromusculaire Nord/Est/Ile de France, Groupe Hospitalier Pitié-Salpêtrière, Paris, France. [5]Sorbonne Université, Inserm, Institut de Myologie, Centre de Recherche en Myologie, F-75013 Paris, France.

[*] **Corresponding author**. Email: salbini@genethon.fr, ORCID: 0000-0001-9502-1004

SUMMARY

The yet incurable Duchenne muscular dystrophy (DMD) is caused by the absence of dystrophin, a protein essential to preserve muscle integrity continuously challenged by contractions. Adeno-associated virus (AAV) delivery of truncated forms of dystrophin is currently the most promising therapeutic approach. However, patient outcomes differed from animal studies, emphasizing the necessity for models predictive of human response. Here, we describe the generation of MYOrganoids, a 3D muscle platform derived from human induced pluripotent stem cells (iPSC), whose structural and functional maturation is enhanced by fibroblasts incorporation. Importantly, a pro-fibrotic microenvironment reproduced by incorporation of dystrophic fibroblasts, was pivotal to exacerbate muscle force loss and fatiguability of DMD MYOrganoids, enabling their use as therapeutic readouts. Remarkably, efficient gene transfer of the gold standard microdystrophin in DMD MYOrganoids, failed to fully restore membrane dystroglycan components and partially rescued muscle strength, in line with the marginal correction of the DMD transcriptional signature achieved. This study highlights the potential of human MYOrganoids to unravel the limitations of current treatments under aggravated conditions and accelerate the discovery of more effective strategies.

Keywords: iPSC, DMD, fibroblasts, MYOrganoids, AAV, microdystrophin

Introduction

Duchenne muscular dystrophy (DMD; ONIM: #310200) is an X-linked disorder that affects one in every 5000 male births [1] with no resolutive cure up to date. It is characterized by progressive muscle wasting affecting skeletal muscles primarily and cardiac and respiratory muscles later, thereby causing premature death [2]. DMD is caused by genetic mutations in the *DMD* gene, leading to the absence of Dystrophin, an essential protein that provides physical support to myofibers by linking them to the extracellular matrix through the Dystrophin Glycoprotein Complex (DGC) [3–6]. The lack of Dystrophin results in a series of muscle membrane breakdowns and repairs, leading to subsequent secondary issues like chronic inflammation and fibrosis [7–10]. Fibrosis, an excessive deposition of extracellular matrix components, is a critical driver of DMD progression. Indeed, secretion of TGFβ (Transforming Growth Factor beta) stimulates the production of matrix components, like fibronectin and collagen, from fibroblasts and myofibers [11–13]

Gene therapy using adeno-associated virus (AAV) is currently the most promising treatment for Duchenne muscular dystrophy. Ongoing clinical trials utilize AAV to deliver short forms of Dystrophin, known as microdystrophin, which encode a truncated but functional protein [14–20]. However, while the therapeutic effects were unequivocally achieved in DMD animal models [21], the results from clinical trials revealed only partial therapeutic efficacy in terms of gain of muscle function, besides the appearance of unexpected safety issues [22,23]. These observations confirm the limited translatability of results obtained in animal models to human patients. It appears therefore crucial to develop high throughput models mimicking human DMD pathology, suitable to quickly assess the efficacy of therapeutics, more reliably and with reduced animal waste and costs. In this context, *in vitro* modeling based on human cells is a valuable option. In particular, the induced pluripotent stem cells (iPSC) technology offers the opportunity to derive an unlimited number of specialized cells from patients for disease modeling and drug screening [24,25]. Among the *in vitro* cellular models, organoid-like structures are becoming invaluable for disease modeling as the use of 3D cultures and biomaterials allows the

reconstitution of tissue architecture and microenvironment that are instrumental for pathophysiological evaluations [26,27].

Although various *in vitro* 3D systems are accessible for modeling Duchenne muscular dystrophy in skeletal muscle engineering [28–31] their throughput use is limited by the long duration and variability related to the complexity of cellular composition achieved. Additionally, the absence of disease-specific readouts for muscle function analysis readouts is still a challenge for assessing the effectiveness of therapeutics. It is also worth noting that tissue engineering applications for AAV gene therapy have been exploited mostly in the context of retinopathies [25,32–34] while only limitedly explored for muscular disorders, for which a high-throughput human muscle system would be an invaluable resource for gene therapy screening.

Here, we described the rapid generation of iPSC-derived muscle organoid-like structure, named hereafter MYOrganoids. We employed and adapted an engineered muscle platform to generate MYOrganoids using a previously reported method for direct iPSC conversion into 2D skeletal muscle cells [35–37]. We further included fibroblasts to increase the structural and functional maturation required for pathophysiological studies. Additionally, we demonstrated that, when DMD-fibroblasts are included, the resulting MYOrganoids display exacerbated pathogenic features related to muscle fragility, making them suitable for studying disease mechanisms and evaluating potential therapeutics. Our study also evaluates for the first time the therapeutic efficacy of AAV-mediated microdystrophin gene transfer, in engineering muscle tissues. As such, while AAV9 infectivity in 3D engineered muscles has been already evaluated [38], in vitro µDys AAV gene transfer, to the best of our knowledge, has not yet been reported. By using different doses of µDys, we observed a dose-dependent response in restoring muscle function and membrane stability in DMD muscles. However, optimal transduction levels resulted in partial recovery of muscle function and at different extent, depending on the derivation of DMD iPSC. This phenomenon mirrors the limited muscle gain observed in treated patients and highlights the varied response of DMD patient-specific muscle tissue to the treatment. Our

findings indicate that patient-derived MYOrganoids, whose pathogenic traits are exacerbated, are suitable for muscle force-based screens and have the therefore the potential to accelerate the identifications of effective therapeutics for DMD in a personalized manner.

Results

Generation of structurally organized 3D human MYOrganoids by direct conversion of iPSC and inclusion of fibroblasts

MYOrganoids were generated from human iPSC committed to differentiating into the myogenic lineage by inducible expression of MyoD and BAF60C [35], from now on referred to as iPSC$^{BM.}$. MYOrganoids were prepared starting from iPSC^{BM} after one day from the induction of myogenic genes. Casting procedure was performed through adaptation of an engineered muscle system [31,39] which results in the growth of the tissue in a ring format supported by two flexible silicon stretchers. The 3D cultures were kept for 2 days in growth medium, afterwards medium was replaced for differentiation for another 12 days (**Figure 1A**). The differentiation protocol was optimized from the conditions previously reported [11,36,37] using myogenic commercial media that ensured the highest expression of myogenic markers and myogenic differentiation in monolayer conditions (**Figure S1A-B**). Since cellular heterogenicity, especially of mesenchymal origin, has been shown to be important for muscle formation [31,40–42], we included human fibroblasts during the casting procedure, to assess whether this would affect muscle organization. For this aim, casting was performed using iPSC^{BM} cells in the presence or absence of human fibroblasts. Achieving alignment and differentiation simultaneously necessitates a delicate balance between fibroblasts and muscle cells (as noted by N. Rao et al., 2013). To replicate physiological conditions accurately, we incorporated a fibroblast concentration that mirrors the stromal population detectable through single cell and single nuclei-RNA seq analysis of muscles [43–46]. We found that including 10% fibroblasts, accelerated the condensation and growth over time of the muscle rings into a compact structure 0.8 mm long and 1 mm thick at day 14 (**Figure 1B).** By performing immunofluorescence in whole-mount tissues for sarcomeric α-actinin (SAA), we could detect an enrichment of SAA-positive myotubes throughout the ring-shaped micro-tissue (**Figure 1C**). We then aimed to assess the impact of fibroblast inclusion on muscle structure. Since the organization of muscle cells within the ECM plays a key role in fusion and maturation [47], both alignment of

myotube and circularity, a consequence of their parallelism, were evaluated. Staining for Myosin Heavy Chain (MyHC, myotube marker) and Vimentin (fibroblasts marker) on longitudinal sections showed fibroblast recruitment near muscle fibers (**Figure 1D**). Myotubes alignment was determined by measuring the angles in between myotubes [48] and showed a significant decrease towards 0 degrees upon fibroblast inclusion, which indicates parallelism while, in the MYOrganoids without fibroblasts, we detected a disordered pattern of muscular cells (**Figure 1E**). Additionally, the circularity of myofibers was measured from transversal sections stained for the membrane marker WGA (wheat germ agglutinin), using the ratio between X and Y Feret diameters (**Figure 1D**). MYOrganoids including fibroblasts had an improved circularity (ratio closer to 1) when compared to control (**Figure 1E**). Improved myotube circularity and alignment as shown, indicate that fibroblast incorporation during the casting procedure, guides skeletal cell orientation providing structural support for MYOrganoids, a prerequisite for maturation.

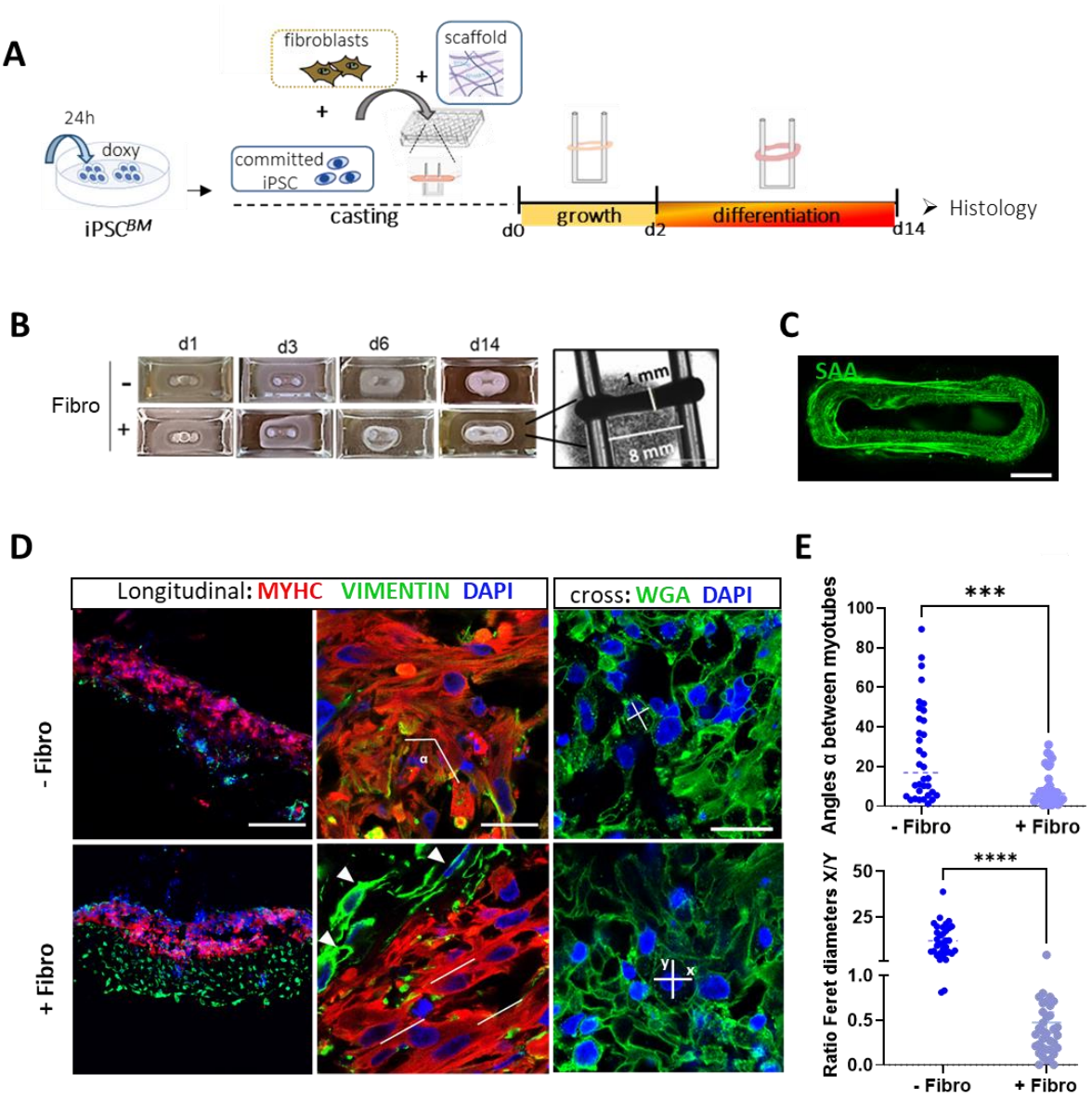

Figure 1. Generation of iPSC-derived MYOrganoids and impact of fibroblast inclusion on muscle organization. ***(A)*** *Scheme of the protocol used to generate muscle artificial tissues (MYOrganoids) from iPSC committed towards the myogenic lineage by 24h treatment with doxycycline for inducible expression of Myod and BAF60C transgenes (iPSC^{BM}). The casting procedure included: committed iPSC, fibroblasts when indicated (+/-fibro) and a collagen-based scaffold, within a 48-well plate equipped with silicon pillars. After 2 days in growth medium, the 3D structures were shifted to differentiation medium until day 14 for histological analysis.* ***(B)*** *Condensation kinetics of MYOrganoids +/-fibro.* ***(C)*** *Whole-mount staining of MYOrganoids with SARCOMERIC α-ACTININ (SAA) and 3D reconstruction of the ring-shaped constructs using confocal imaging. Scale bar: 1 mm.* ***(D)*** *Representative longitudinal and cross sections of MYOrganoids +/- fibroblasts, immunostained for Myosin Heavy Chain (MYHC) and VIMENTIN or for wheat germ agglutinin (WGA). Nuclei were visualized with DAPI. Scale bars 200 µm (left panel) and 10 µm (middle and right panel). Arrows indicate fibroblasts recruited adjacently to the muscle fibers; α is the angle formed between myotubes; lines indicate aligned myotubes, crosses represent X/Y myotubes diameters.* ***(E)*** *The alignment was calculated based on the angle (α) formed between myotubes (α close to 0 corresponds to aligned myotubes, while far from 0 corresponds to not aligned myotubes), while circularity from X/Y myotubes diameters ratio (ratio 1 circular, far from 1 not circular). Data were collected from 3 independent experiments with at least 3 replicates. N=35. Unpaired two-tailed t-test was used (***$p \leq 0.001$, ****$p \leq 0.0001$).*

Increased structural and functional maturation of fibroblast-including MYOrganoids

Since muscle maturation is strictly dependent on the internal myofiber organization, we evaluated the differentiation of our 3D MYOrganoids by looking at the sarcomere structure. Transversal and longitudinal sections were used to monitor Dystrophin (DYS) expression at the sarcolemma **(Figure 2A**) and sarcomeric α-actinin (SAA) localization for assessment of the striation pattern typical of mature myotubes (**Figure 2B**). Dystrophin was properly localized to the muscle membrane of myotubes from MYOrganoids including fibroblasts and was significantly more expressed compared to MYOrganoids without fibroblasts (**Figure 2D**). Remarkably, the maturation index, reported as a percentage of the number of nuclei included in striated myotubes, was significantly superior in MYOrganoids including fibroblasts as compared to MYOrganoids without fibroblasts which appear very disorganized with a rare appearance of striations (**Figure 2E**). Increased maturation of myotubes within MYOrganoids including fibroblast was also supported by analysis of the fusion index, indicating a significantly higher percentage of multinucleated myotubes (>3 nuclei) and a lower percentage of mononucleated ones. This evidence highlights the positive role of fibroblasts in the maturation process through fusion and multinucleation (**Figure 2F**). The proper sarcomeric organization was also confirmed by electron microscopy where we could detect longer, properly formed Z patterning and the presence of I and A bands along with an overall increase of sarcomeric density and alignment (**Figure 2C**). Consistently, MYOrganoids containing fibroblasts showed wider Z-line (**Figure 2H**), index of higher maturation of sarcomeres [49]. We further performed gene expression analysis for terminal differentiation markers such as muscle creatine kinase (*MCK*), myosin heavy chain (*MYH*) isoforms, such as *MYH2*, representative of fast adult fiber type, and *MYH7*, as a slow fibers marker (**Figure 2G**). Higher expression of all genes in MYOrganoids containing fibroblasts confirms the acquisition of a more mature state, compared to MYOrganoids without fibroblasts.

We then assessed whether our MYOrganoids were functional by evaluating their physiological response to contraction stimulations, using a muscle organ bath system based on electrical pacing [50]. To evaluate muscle force, MYOrganoids were transferred to the muscle strip chamber and stretched until the optimal length (Lo) for functional analysis (**Figure 2I**). Isometric force analysis revealed significantly higher tetanic force in MYOrganoids containing fibroblasts compared to the control (**Figure 2J**). Values were then normalized for the cross-sectional area (CSA) using the weight and optimal length of contraction established for each MYOrganoid [51,52] and expressed as specific tetanic force (mN/mm^2) (**Figure 2K**). In particular, the highest force with fibroblasts had peak values ranging from 0.3 to 0.5 mN versus 0.1 to 0.2 mN in MYOrganoids without fibroblasts after normalization (**Figure 2K**). These data demonstrated that MYOrganoids plus fibroblasts have an improved structural organization and functional maturation that enables force contraction studies by electrical pacing.

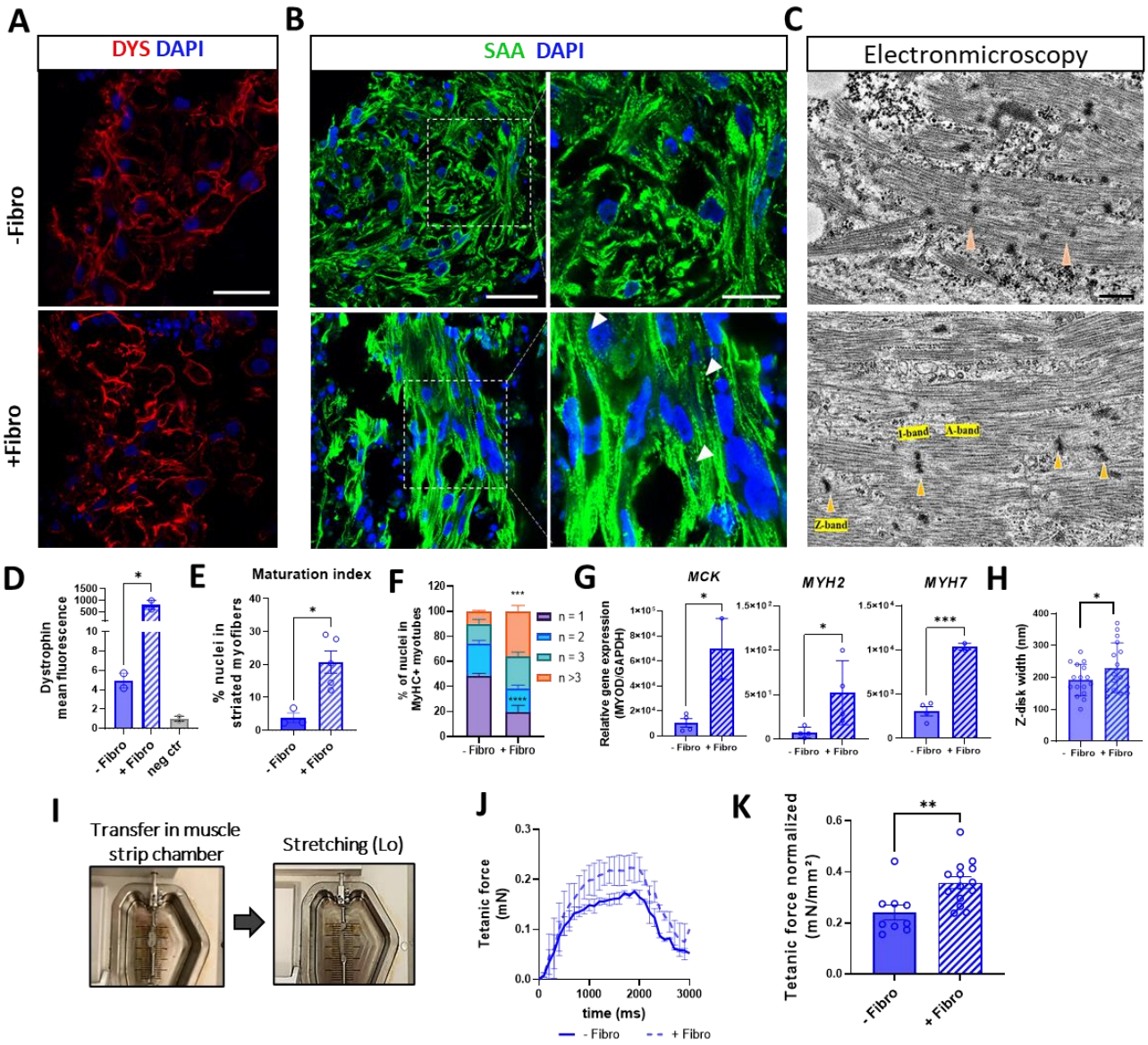

157

158

Figure 2. Structural and functional maturation in fibroblast-including MYOrganoids. (A) *Representative transversal sections stained for DYSTROPHIN (Dys). Scale bar: 40 µm. Nuclei were visualized with DAPI.* ***(B)*** *Representative longitudinal sections of MYOrganoids +/- fibroblasts (fibro), immunostained for SARCOMERIC α-ACTININ (SAA). Scale bars: 40 µm, enlargement 10 µm.* ***(C)*** *Transmission electron microscopy images showing sarcomeric structures. Orange arrows: Z-lines. Scale bar: 500 nm.* ***(D)*** *DYSTROPHIN staining quantification represented as mean intensity fluorescence and expressed as fold change to the negative control (sections stained without first antibody). N=2* ***(E)*** *Quantification of maturation index was performed by calculating the nuclei inside striated myofibers visualized by SAA staining as a percentage of the total number of myofibers. N=3-5* ***(F)*** *Quantification of fusion index calculated as % MYOSIN HEAVY CHAIN positive (MYHC+) myotubes containing different numbers of nuclei (n) as depicted. N=3* ***(G)*** *Gene expression analysis of MCK, MYH2 and MYH7, reported as gene expression relative to MYOD expressing population. N=2-5* ***(H)*** *Width of Z-line visualized by Electron microscopy, in MYOrganoids with and without inclusion of fibroblasts. N=16* ***(I)*** *Contractile muscle force analysis of MYOrganoids using a muscle-strip-based organ bath system. Lo, the optimal length used for normalization of force data (see methods).* ***(J)*** *Representative tetanic traces of MYOrganoids with and without the inclusion of fibroblasts. N=3* ***(K)*** *Normalized tetanic force peak in MYOrganoids +/- fibroblasts. N=8-15). Data are presented as means +/- SEM. Unpaired t-test was applied for statistical analysis (*p ≤0.05, **p ≤ 0.01, ***p ≤ 0.001, ****p ≤ 0.0001).*

DMD iPSC-derived MYOrganoids including fibroblasts display exacerbated pro-fibrotic activity

The improved muscle organization and functional maturation shown by MYOrganoids including fibroblasts, prompted us to exploit fibroblast features in disease modeling for DMD, where their role in disease progression is well known [12,13]. As such, fibroblasts and ECM compose the connective tissue which is a key regulator of differentiation and muscle structure as well as of the muscle niche that undergoes pathological remodeling during disease [41,42]. In this context, fibroblasts play a major role in muscle assembly and act as a source of microenvironment cues exerted by their secretory activity [41,52–54]. We incorporated DMD fibroblasts as a means to recapitulate the pathogenic microenvironment arising from their profibrotic activity exerted by tissue remodeling and matrix deposition [13,55]. For that purpose, we used three DMD iPSC with different *DMD* mutations, a deletion of exon 45 (DMDdEx45), a deletion of exons 8-43 (DMDdEx8-43) and a deletion of exons 8-9 (DMDdEx8-9) with their isogenic control, the DMD dEx8-9 iPSC corrected to restore dystrophin expression [56] (hereafter called corrDMD dEx8-9). We additionally used two control iPSC lines derived from healthy patients (Ctr1, Ctr2). Control and DMD MYOrganoids were generated from control and DMD iPSC together with human healthy or DMD immortalized fibroblasts for histological and molecular analyses (**Figure 3A**). The myogenic differentiation ability of both Ctr and DMD iPSC lines was first evaluated in 2D cultures. All cell lines showed comparable differentiation potential, as expected using a direct myogenic conversion protocol bypassing any defective developmental steps (**Figure S2A**). Histological characterization in MYOrganoids, showed the absence of Dystrophin protein in DMD MYOrganoids and efficient myogenic differentiation and maturation in Ctr and DMD MYOrganoids, as shown by the striated pattern visualized by SAA-stained sections, confirming the positive role of fibroblasts in enhancing maturation also in a DMD context (**Figure 3B**). We then monitored fibrotic hallmarks at the histological level by looking at FIBRONECTIN (FN1), one of the major TGFβ target ECM genes and phosphorylated SMAD3 (pSMAD3), the transcriptional effector of canonical TGFβ pathway. Notably, DMD MYOrganoids from all DMD iPSC, including DMD fibroblasts showed

increased expression of FIBRONECTIN and increased number of pSMAD3 positive nuclei, indicating activation of TGFβ in DMD MYOrganoids and fibrosis, as compared to Ctr MYOrganoids (**Figure 3C-D**). The presence of fibrosis within the DMD MYOrganoids was also confirmed by the increased mRNA expression of FIBRONECTIN1 (*FN1*) and COLLAGEN1 (*COL1A1*) (**Figure 3E-F**). Remarkably, the differences in the expression of fibrotic markers between Ctr and DMD MYOrganoids were significant only when including fibroblasts (**Figure 3C-F**). The presence of a fibrotic environment of DMD MYOrganoids was also confirmed by an increase in Collagen IV released in the media of DMD MYOrganoids, as compared to Ctr MYOrganoids, which was significantly higher in the condition including fibroblasts (**Figure S2B**).

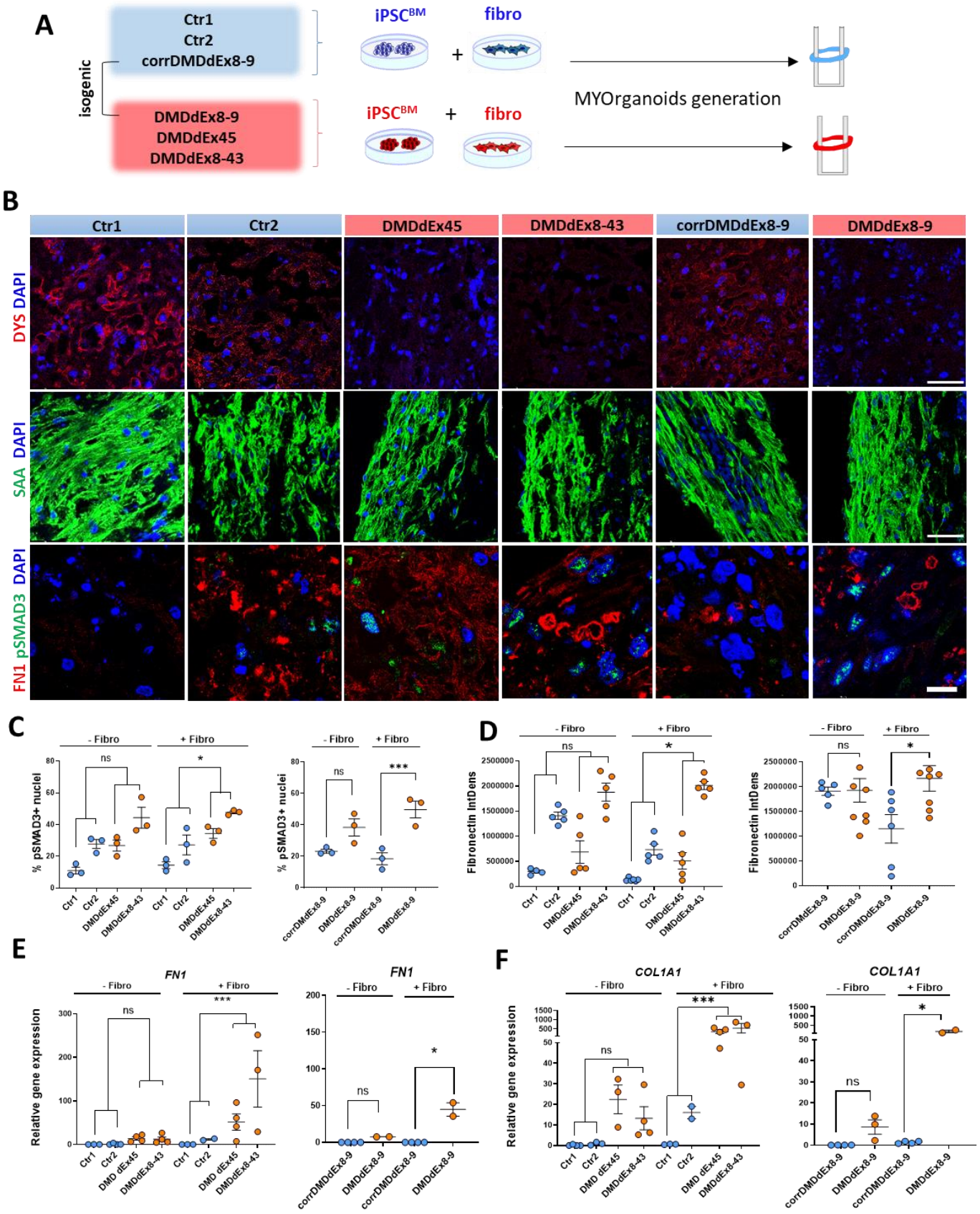
A
isogenic
Ctr1
Ctr2
corrDMDdEx8-9
DMDdEx8-9
DMDdEx45
DMDdEx8-43
iPSC^BM
fibro
MYOrganoids generation
B
Ctr1
Ctr2
DMDdEx45
DMDdEx8-43
corrDMDdEx8-9
DMDdEx8-9
DYS DAPI
SAA DAPI
FN1 pSMAD3 DAPI
C
% pSMAD3+ nuclei
- Fibro
+ Fibro
ns
*
***
D
Fibronectin IntDens
E
FN1
Relative gene expression
F
COL1A1

Figure 3. DMD iPSC-MYOrganoids including DMD fibroblasts exacerbate pathogenic hallmarks. (A) *Overview of MYOrganoids generation from control iPSC (Ctr1 and Ctr2), DMD iPSC (DMDdEx45, DMDdEx8-43) and isogenic iPSC (corrDMDdEx8-9 and DMDdEx8-9) including Ctr or dystrophic fibroblasts respectively for histological characterization and gene expression analysis.* ***(B)*** *Immunostaining of MYOrganoids cross sections for DYSTROPHIN (Dys) and SARCOMERIC a-ACTININ (SAA), Scale bar: 40 µm, or for SARCOMERIC α-ACTININ (SAA) and FIBRONECTIN (FN1)/pSMAD3 in longitudinal sections. Scale bar: 40 µm and 20 µm, respectively.* ***(C)*** *Quantification of % of pSMAD3 positive nuclei in all Ctr and all DMD MYOrganoids. N=3 (**D**) Quantification of FIBRONECTIN fluorescence signal in all Ctr and DMD MYOrganoids. N=3* ***(E-F)*** *RT-ddPCR analysis of fibrotic markers Fibronectin 1 (FN1) (**E**) and Collagen 1 (COL1A1) (**F**) in all Ctr and all DMD iPSC-derived MYOrganoids with or without fibroblast. Isogenic cell lines are represented in a separate graph. N=2-4. Data are presented as mean ± SEM. Unpaired t-test was performed for statistical purposes (*p ≤0.05, **p ≤ 0.01, ***p ≤ 0.001, ****p ≤ 0.000), ns= not significant.*

Disease exacerbation by fibroblast incorporation reveals muscle strength loss and fatiguability of DMD MYOrganoids

To assess whether DMD MYOrganoids display hallmarks of DMD pathophysiology, we evaluated muscle function, which represents one of the most difficult challenges in the establishment of therapeutic readouts with *in vitro* systems. To identify reliable force parameters reflecting the defective DMD muscle performance, MYOrganoids were subjected to isometric contractions (ISO) to measure tetanic force (**Figure S2C**), and to eccentric contractions (ECC) to assess muscle strength and fatiguability (**Figure 4**). In line with the facts that MYOrganoids have never been challenged neither by contraction nor stretching at the time of functional evaluation and have the same myogenic potential and maturation (**Fig S2A and Fig 3B**), we did not observe a consistent change in the tetanic force between Ctr and DMD MYOrganoids, regardless of fibroblast incorporation (**Figure S2C**). As eccentric contraction plays a critical role in the disease progression of DMD [57] and repeated contractions trigger the degeneration/regeneration cycles [58], we used a specific eccentric repetition protocol to assess muscle force loss and resistance under exhaustion. The protocol consisted of ten repetitions of eccentric contractions, where the force developed after each lengthening was calculated to trace muscle force drop over time. The drop force in all the DMD iPSC-derived-MYOrganoids upon ten consecutive eccentric contractions was significantly higher than in control MYOrganoids and the corrected isogenic cell line (corrDMDdEx8-9) including fibroblasts starting from the 4th eccentric

repetition (**Figure 4A**). On the other side, Ctr and DMD MYOrganoids not including fibroblasts, show significant differences in drop force just at the tenth repetition (**Figure 4B**). To accurately quantify muscle fatigue, we calculated the fatigue index as the drop of force between the isometric contractions performed before and after the 10 repetitions of eccentric exercise. The analysis showed a significantly higher fatigue index in DMD MYOrganoids as compared to Ctr MYOrganoids and remarkably, this phenomenon was highly accentuated by the presence of fibroblasts. (**Figure 4C)**. We then checked whether the impact on disease exacerbation and increase of difference in fatiguability between Ctr and DMD MYOtissue was affected by the different genetic backgrounds of the fibroblast source, we employed three additional fibroblast cell lines from either healthy and DMD individuals to generate Ctr and DMD MYOrganoids. Muscle force analysis confirmed that the fatigue index in DMD MYOrganoids was significantly higher than Ctr MYOrganoids, regardless of the genetic source of either control or DMD fibroblasts. This analysis also confirmed the higher significance of muscle fatigue index comparison from fibroblasts-including MYOrganoids as compared to the difference observed between Ctr and DMD MYOrganoids without fibroblasts (**Figure 4D**). This evidence supports the potential of using fibroblasts in tissue engineering as a source of ECM and pro-fibrotic cues under pathological conditions. Collectively these data indicate that DMD MYOrganoids including DMD fibroblasts, through their pro-fibrotic activity, display exacerbated loss of muscle resistance and increase in fatiguability (**Figure 4A-D)**, thereby defining pro-fibrotic DMD MYOrganoids as the most appropriate system for further analysis. The finding also demonstrates that eccentric-based drop force evaluation is a meaningful and reliable therapeutic readout, as significant differences were detected between Ctr and DMD MYOrganoids including fibroblasts.

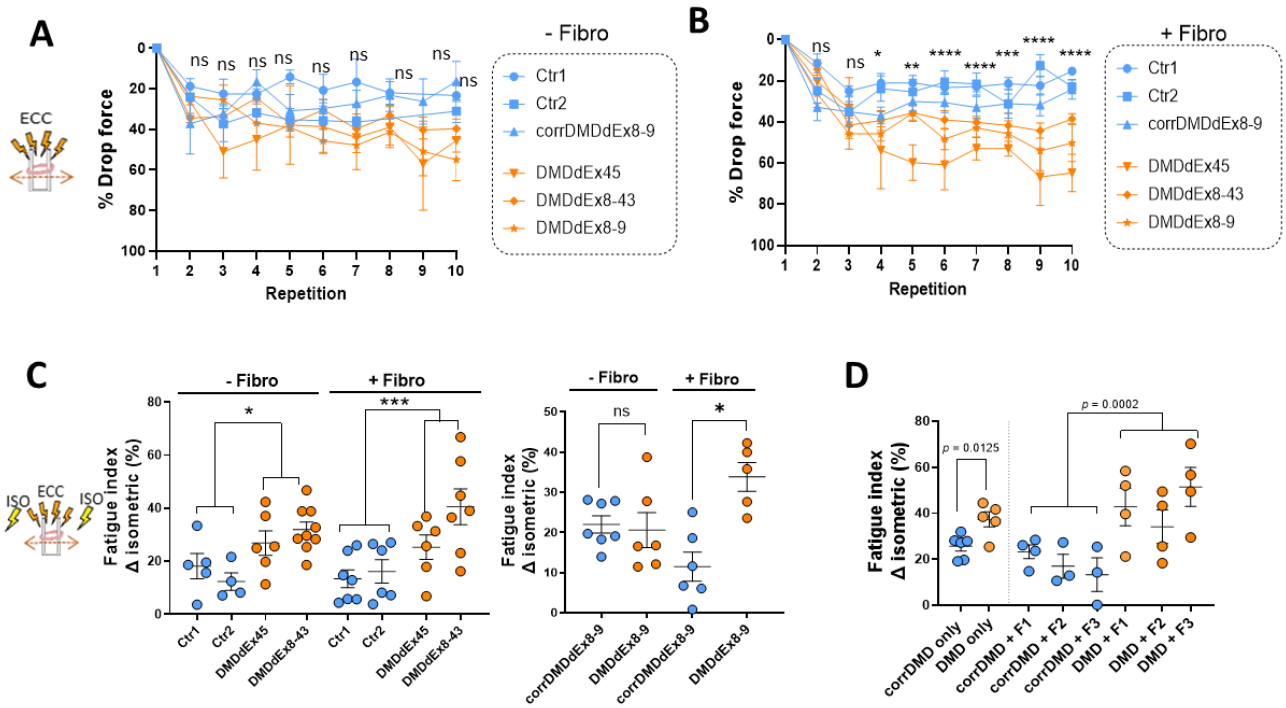

Figure 4. Significant muscle force loss and reduced endurance in DMD MYOrganoid including dystrophic fibroblasts. ***(A-B)*** *Force drop over 10 repetitions of eccentric (ECC) contractions in all Ctr and all DMD MYOrganoids without* ***(A)*** *or with fibroblasts* ***(B)*** *N=4-6.* ***(C)*** *Fatigue index calculated as % of drop force between two ISO performed before and after 10x repetitions of* ECC *in all Ctr and all DMD MYOrganoids +/- respective fibroblasts. N=5-10* ***(D)*** *Fatigue index, in corrDMDdEx8-9 and DMDdEx8-9 MYOrganoids +/- three Ctr and DMD fibroblasts obtained from different genetic sources. N=3-6 Data are presented as mean ± SEM. Unpaired t-test was performed for statistical purposes (*p ≤0.05, **p ≤ 0.01, ***p ≤ 0.001, ****p ≤ 0.000), ns= not significant.*

Microdystrophin gene transfer improves muscle strength and fatiguability

As proof of concept that MYOrganoids were suitable as a screening platform for gene therapy, we used AAV-mediated delivery of microdystrophin (µDys) and assessed its therapeutic efficacy in the DMD context by performing firstly muscle force analysis. For this aim, we used AAV9, as this serotype was used in recent clinical trials and showed high transduction rate in patients' myofibers [59,60]. We first optimized the infection conditions using the reporter AAV9-CMV-GFP in Ctr MYOrganoids including fibroblasts. Infection was performed on day 7 of the differentiation protocol, diluting AAV particles directly in the medium, and maintained for an additional 7 days (**Figure S3A-C**). We then used a codon-optimized microdystrophin gene (dR4-23) under the control of the muscle-specific sp512 promoter [17] for gene transfer using AAV9 (AAV9-µDys) in all DMD MYOrganoids iPSC (dEx45, dEx8-43 and dEx8-9 with isogenic control-crrDMDdEx8-9) (**Figure 5A**). This construct leads to the

same protein product used in clinical trials [61]. Low and high doses were established based on previous dosing studies to have intermediate transduction levels at low doses (1^9 vg/MYOtissue), and high transduction levels at high doses (5^10 vg/MYOtissue) (**Figure S3D**). Gene transfer efficiency was evaluated by quantification of Viral copy number (VCN) on genomic DNA and by the expression level of the transgene and the encoded protein, in Ctr and DMD MYOrganoids (**Figure 5B-D, Figure S4A-B**). A clear dose-dependent entry of µDys increase of DNA, mRNA, and protein levels was detected following AAV9-µDys gene transfer in DMD MYOrganoids obtained from all DMD iPSCs. Interestingly, isometric tetanic force analysis did not reveal any significant increase in DMD MYOrganoids following µDys delivery compared to non-infected conditions (**Figure 5E**). As seen before, this result is expected considering the muscle tissue has never experienced contraction at the time of gene transfer. The contraction-induced membrane damage may be therefore necessary to reveal the pathogenic phenotype and the effect of µDys. We then challenged the muscles with repeated eccentric repetitions, and, under this condition, we observed a dose-dependent attenuation of the drop force in DMD MYOrganoids (**Figure 5G**). Consistently with the increased muscle strength, the fatigue index was greatly reduced in a dose-dependent manner in all DMD MYOrganoids treated with a high dose of µDys, although reaching significance only for DMDdEx45 and DMDdEx8-9 MYOrganoids (**Figure 5F**). The results of muscle force rescue upon µDys gene transfer were further confirmed using an inactive vector as a control to rule out nonspecific effects due to AAV delivery (**Figure S4D-H**). Overall, these data confirmed that ectopic µDys exert a positive function in the rescue of muscle endurance, although at different extent among the DMD iPSC-derived MYOrganoids.

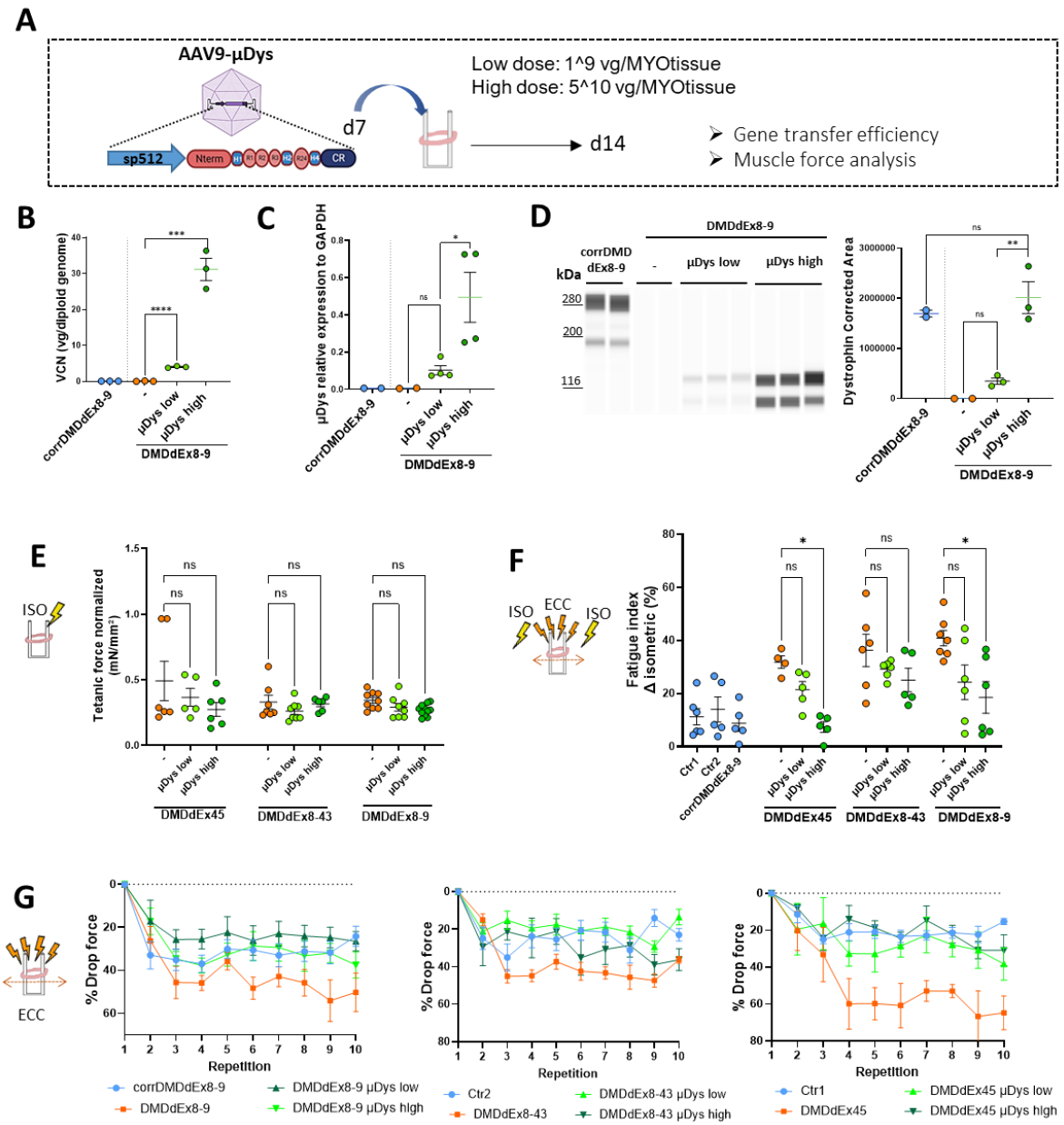

266

Figure 5. Muscle strength evaluation following AAV-mediated delivery of µDys in profibrotic DMD MYOrganoids. *(**A**) Scheme of AAV9-µDys infection and doses used in DMD iPSC-derived MYOrganoids. (**B-C-D**) Evaluation of gene transfer efficiency by Viral copy number (VCN) analysis (N=3) **(B)**, mRNA expression levels (N=2-4) **(C)** and protein expression analysis by capillary western blot in the representative isogenic iPSC DMD dEx8-9-derived MYOrganoids infected with low and high dose of µDys versus non-infected (-) corrDMDdEx8-9 (N=2-3) **(D)**. **(E)** Tetanic force in all DMD iPSC-derived MYOrganoids, treated with µDys and subjected to a first isometric contraction. **(F)** Fatigue index in all Ctr and DMD MYOrganoids treated or not with m-Dystrophin at low and high dose. N=5-6. **(G)** Drop force over 10 repetitions of eccentric (ECC) contractions in isogenic cell lines and Ctr1, Ctr2 and DMDdEx45, DMDdEx8-43-derived MYOrganoids receiving low and high doses of µDys. N=6-7. Data are presented as means +/- SEM. Statistical analysis was performed with an ordinary one-way ANOVA test (*p ≤0.05, **p ≤ 0.01, ***p ≤ 0.001, ****p ≤ 0.0001, ns = not significant) with multiple comparisons corrected with Tukey's test.*

AAV-microdystrophin gene transfer in pro-fibrotic DMD MYOrganoids fails to restore Dystrophin Glycoprotein Complex components and partially reduces the inflammatory milieu

Because dystrophin exerts its biomechanical support by holding the Dystrophin Glycoprotein Complex (DGC) in place, we monitored key components of this complex, the transmembrane β-Dystroglycan (β-DG), directly binding Dystrophin, and the extra-cellular α-Dystroglycan (α-DG), binding β-DG, whose proper expression and localization are impaired in the absence of Dystrophin [62]. To this aim, DMD MYOrganoids infected with low and high dose of µDys, were subjected to both histological and secretome analysis to evaluate membrane stability (**Figure 6A**). Histological quantification of µDys showed around 25-30% of dystrophin-positive myotubes at low dose compared to 85% in the high dose condition in DMD dEx8-9 and dEx45 and a 65% in the DMD dEx8-43 MYOrganoids (**Figure 6B,** top panel, and **S4**). Immunostaining on transversal MYOrganoids showed a dose-dependent yet not complete restoration of β-DG in all DMD iPSC-derived MYOrganoids (**Figure 6B** and **S5**). Interestingly, even high doses ensuring nearly total Dystrophin transduction in all the DMD MYOrganoids did not significantly restore α-DG (around 10% in DMDdEx8-9 and DMDdEx8-43 and around 30% in DMDdEx45) suggesting a potential therapeutic limitation of µDys. Importantly, these data demonstrate the limited restoration of Dystrophin-associated components to the sarcolemma after successful µDys gene transfer. To understand the effect of the partial DGC restoration on membrane stability, we looked at the inflammatory response, a key pathogenic hallmark in damaged dystrophic muscle, that is mediated by proinflammatory cytokine release by myofibers and fibroblasts upon mechanical stress. For this aim, pro-fibrotic DMD MYOrganoids treated or not with µDys were subjected to secretome analysis to assess production of Interleukin 8 (IL-8), Interleukin 6 (IL-6) and Tumor Necrosis Factor-alpha (TNFα), [9,63] from conditioned media collected 24h after the eccentric contraction (**Figure 6A)**. Remarkably, secretion of the three factors decreased in a dose-dependent manner upon µDys restoration, although it was significant only in DMD dEx45-derived MYOrganoids. Moreover, IL6 production was not significantly counteracted in none of the DMD

iPSC-derived MYOrganoids (**Figure 6D**). These data confirmed that, upon µDys restoration in DMD organoids, only a partial improvement of the membrane stability and inflammatory milieu is achieved.

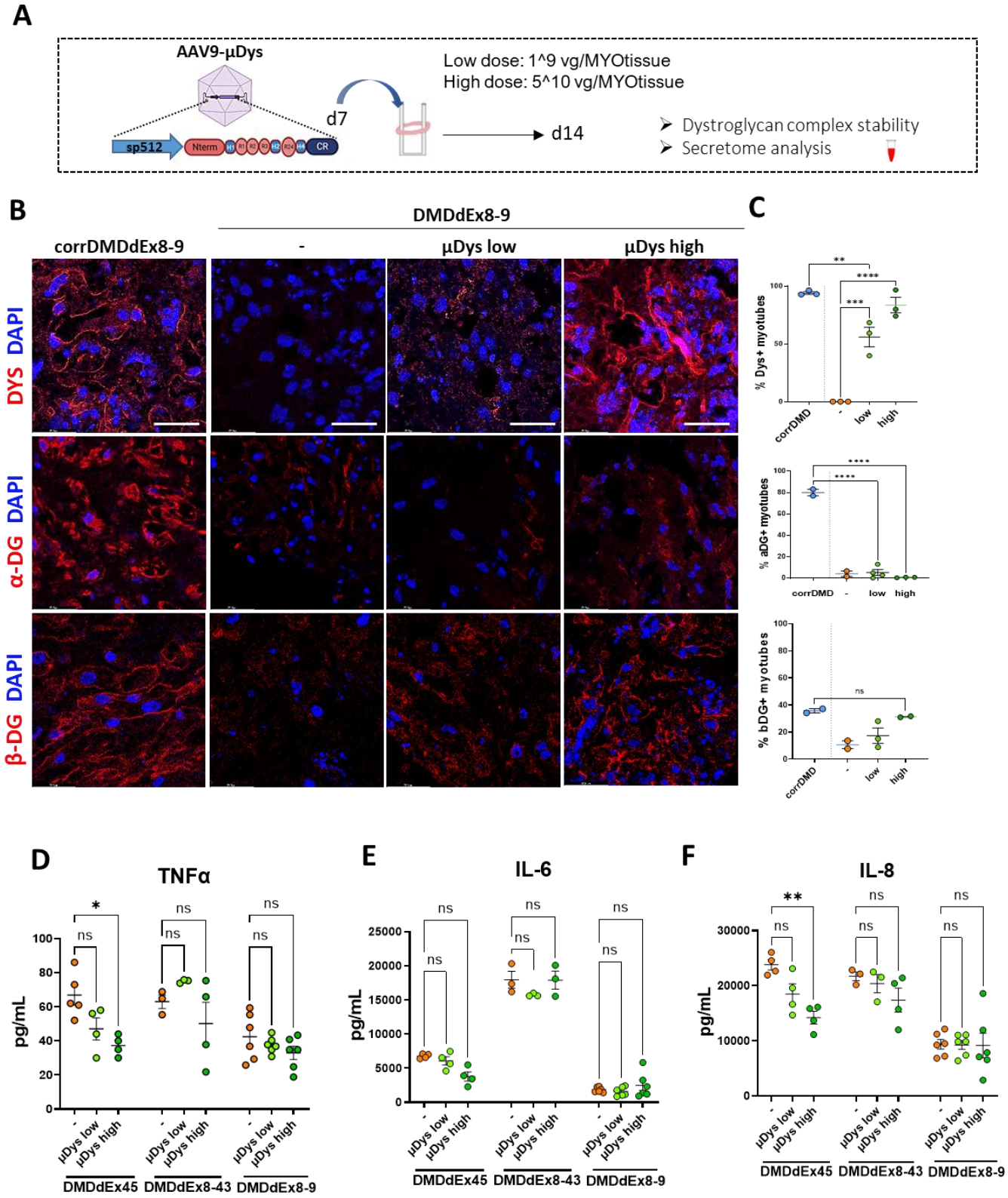

Figure 6*. Restoration of DGC members and secretome analysis following microdystrophin gene transfer.** *(**A**) Ctr and Scheme of control and DMD MYOrganoids subjected to muscle force assessment and secretome analysis following AAV-µDys gene transfer.* ***(B) *Histological evaluation of Dystrophin Glycoprotein Complex (DGC) upon infection, by immunostaining for Dystrophin (Dys), α-Dystroglycan (α-DG) and β-Dystroglycan (β-DG**)** of Ctr and DMD cross sections of MYOrganoids. Images are relative to the representative isogenic iPSC. Scale bar: 40 µm.* ***(C)*** *DYSTROPHIN (DYS), α-DYSTROGLYCAN (α-DG) and β- DYSTROGLYCAN (β-DG**)** quantification in DMDdEx8-9 iPSC-MYOrganoids cross sections and its isogenic corrected control (corr), N=3-6.* ***(D-F)*** *Quantification of TNFα (**D**), IL-6 (**E**) and IL-8 (**F**) cytokines released in the media collected 24h after eccentric training. N=4-5. Data are presented as mean ± SEM. Statistical analysis was performed with unpaired t-test (*p ≤0.05, **p ≤ 0.01, ***p ≤ 0.001), ns=not significant*

Optimal microdystrophin gene transfer partially corrects the transcriptomic profile of DMD MYOrganoids

To examine the effect of the absence of dystrophin on the signaling pathway and molecular process contributing to the dystrophic pathology and assess whether they were restored by µDys gene transfer, we performed bulk RNA-seq analysis comparing firstly the corrected DMD dEx8-9 (isogenic control/corrDMD) and DMDdEx8-9 MYOrganoids and then, the DMDdEx8-9 untreated and treated with high dose of AAV9-µDys (n=4).

Principal component analysis (PCA) of the top 10000 genes with the highest variance showed a distinct transcriptomic profile of DMD organoids compared to isogenic controls. Additionally, µDys-treated MYOrganoids did not cluster closer to corrected isogenic organoids (Figure **S6A**). Consistently, a clustered heatmap of all 1716 most significant differentially expressed genes (DEGs) further highlighted the transcriptomic differences between corrected and DMD organoids, as well as a variegated pattern of expression profile after µDys gene transfer (**Figure 7A**). Compared to isogenic control, DMD organoids presented 4610 DEGs, of which 2181 upregulated and 2429 downregulated (**Figure S6B**). Gene ontology enrichment analysis between DMDdEx8-9 versus corrDMD organoids revealed the presence of dysregulated biological processes typical of DMD, such as downregulation of muscle contraction, mitochondrial respiratory chain, ATP production, oxidative

phosphorylation, calcium ion transport, and sarcomeric organization (**Figure 7B and S6C**). In addition, upregulation of collagen organization process was found upregulated, in agreement with our exacerbation of matrix remodeling.

To evaluate the effect of µDys in restoring key pathways involved in DMD, we firstly compared the transcriptomic profile of µDys-treated DMD organoids to untreated DMD organoids (dEx8-9 µDys vs dEx8-9), and then to the isogenic control (dEx8-9 µDys vs corrDMD). Particularly, µDys-treated DMD organoids showed a total of 327 DEGs, of which 154 upregulated and 173 downregulated, compared to untreated organoids (**Figure 7C**). Of those 327 DEGs, 52% (170/327) are in common with the DEGs that were found dysregulated in DMD organoids when compared to the isogenic control (**Figure S6D**). Therefore, we performed the gene ontology enrichment analysis of the common category to see the effect of uDys on the DMD-dysregulated pathways (**Table S1**). This analysis revealed decreased expression of genes involved in the ECM remodeling (GOBP: Collagen catabolic process), such as collagens and laminins, and inflammation (GOBP: Regulation of inflammatory response). Conversely, we found an upregulation of genes involved in microtubule organization, (GOBP: Microtubule organizing center organization) involved in the mechanotransduction-dependent pathway (**Figure 7D**).

However, not all DEGs were significantly corrected when compared to the isogenic control (corrDMD). In particular, µDys-treated organoids present 7818 DEGs (4004 upregulated and 3814 downregulated) when compared to the corrected isogenic organoids (**Figure 7E**). Gene ontology analysis of the DEGs between µDys-treated DMD organoids and corrDMD organoids revealed the pathways that are not restored by the gene transfer. Particularly, treated organoids presented a downregulation of genes involved in calcium transport (GOBP: Sarcoplasmic reticulum calcium ion transport), oxidative phosphorylation (GOBP: Oxidative phosphorylation) and skeletal muscle contraction (GOBP: Actin myosin filament sliding) when compared to isogenic controls (**Figure 7F**).

These data demonstrate that the optimal gene transfer of µDys in DMD MYOrganoids normalizes only a small portion of the dysregulated transcriptome, leaving several key pathogenic pathways still dysregulated after the gene transfer.

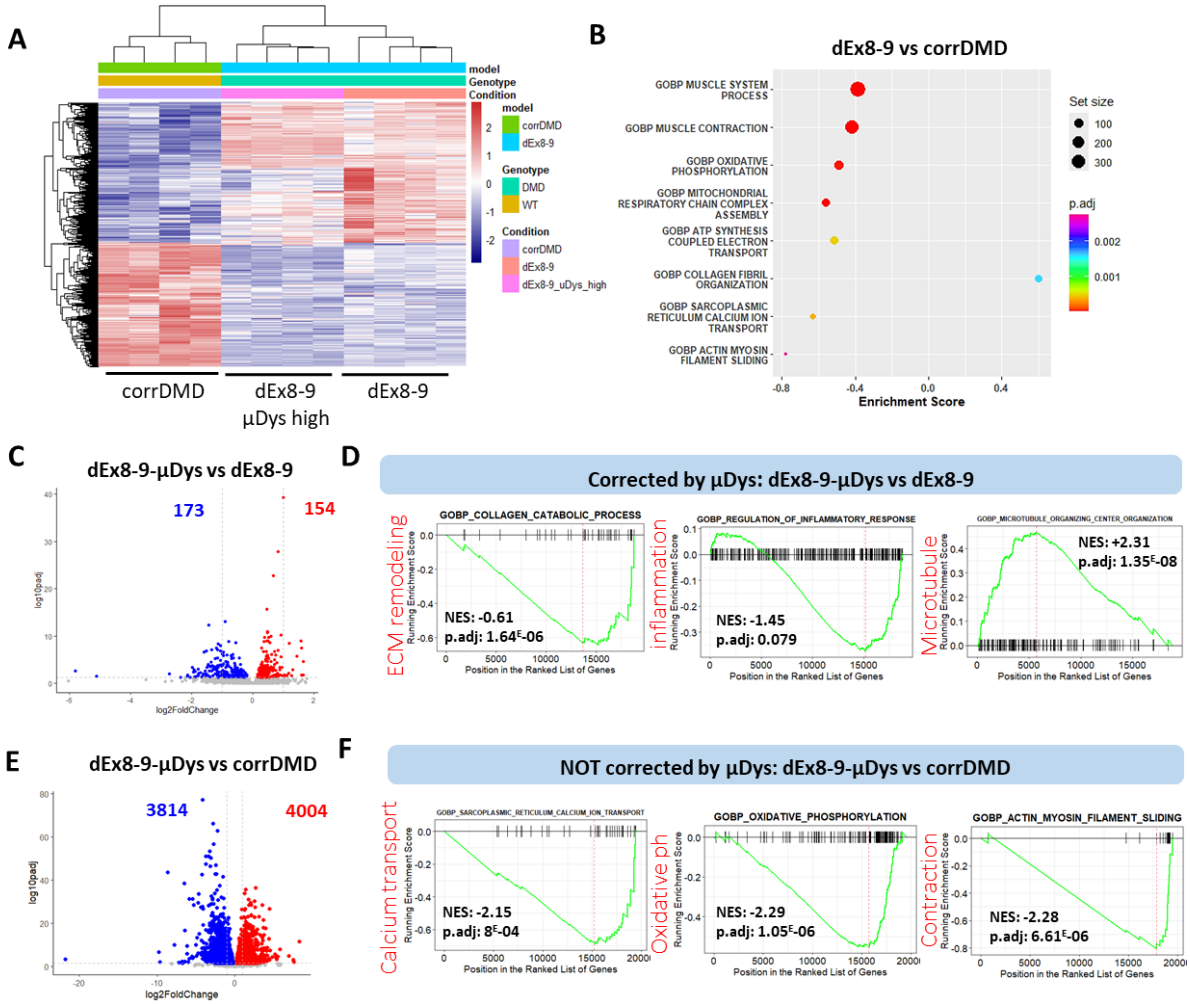

Figure 7: Transcriptomic analysis in µDys-treated isogenic DMD MYOrganoids. (A) *Clustered Heat map depicting relative transcript levels of differentially expressed genes in corrected DMD (corrDMD) and DMD MYOrganoids transcriptomics treated or not with µDystrophin (dEx8-9 and dEx8-9 µDys high). Lower and higher expressions are depicted in blue and red, respectively.* ***(B)*** *Dot plot of specific pathways depicted by gene ontology enrichment analysis of all significantly upregulated and downregulated genes in DMD MYOrganoids (dEx8-9) compared to isogenic control (corrDMD).* ***(C)*** *Volcano plot showing the differential gene expression in treated (dEx8-9-µDys) versus untreated (dEx8-9) DMD MYOrganoids. Upregulated genes are shown in red, while downregulated genes are shown in blue. Numbers indicate the amount of downregulated and upregulated genes* ***(D)****Gene ontology enrichment analysis of treated (dEx8-9-µDys) versus untreated (dEx8-9) DMD MYOrganoids. Normalized enrichment score (NES) and adjusted p value (p.adj) are indicated for each subcategory.* ***(E)*** *Volcano plot showing the differential gene expression in DMD MYOrganoids treated with µDystrophin (dEx8-9-µDys) vs isogenic control (corrDMD). The data points above the significance threshold (p adjusted < 0.05, fold2change > 2) are marked in blue*

*(downregulated) and red (upregulated), and others are marked in gray (not significant). (**F**) Gene ontology enrichment analysis of treated (dEx8-9-µDys) versus isogenic control (corrDMD) MYOrganoids. Normalized enrichment score (NES) and adjusted p value (p.adj) are indicated for each subcategory.*

Discussion

The investigation and identification of new therapeutic strategies to face DMD are hampered by the lack of disease models resembling human pathology and enabling muscle function evaluation in a high-throughput fashion. Here, we report the generation of 3D engineered muscles called MYOrganoids, composed of a homogeneous population of myogenic cells derived from direct conversion of iPSC [11,36] combined with fibroblasts, within a collagen-based matrix. We included fibroblasts during MYOtissue generation, at the physiological ratio as compared to muscle cells, as they are the major component of the surrounding connective tissue required for self-assembly and maturation of the myofibers [41,42,53]. This resulted in a mature muscle structure and high functional performance under muscle force evaluation.

Our system offers a distinct advantage in its ability to analyze muscle resistance and fatigue. While several remarkable studies reported on muscle force in 3D models [30,31,56,64,65], evaluating muscle function still presents challenges due to the complexity of identifying disease-specific force parameters and the variability of in vitro models. Here we established parameters to evaluate muscle strength and fatigue index, defined as resistance to repeated eccentric contractions [66]. Notably, the use of our direct differentiation methods, enabled us to perform muscle force analysis without bias introduced by either intrinsic myogenic defects or by heterogenous populations that may affect muscle force analysis [31,49,67]. Importantly, we incorporated fibroblasts to replicate the profibrotic activity in a DMD muscle context, which greatly contributes to establishing the pathogenic dystrophin niche, characterized by excessive and persistent ECM remodeling and inflammation. This strategy allows simulation of the increase in rigidity of DMD muscle fibers which consequently leads to an increase of susceptibility to

contraction-induced damage and fatigue. While our approach relies on the use of non-isogenic fibroblast cell lines to generate MYOrganoids, we demonstrated that our results were not significantly affected by the genetic background of these cells. This evidence points to a dominant role of the function of the fibroblast exerted by their secretory activity, thereby supporting the potential of this cellular strategy. Overall, the exacerbated severity of DMD MYOrganoids allows gaining a broader window to evaluate the therapeutic potential of AAV gene therapy products.

Finally, our system, being based on direct myogenic conversion without formation of muscle stem cells, presents the opportunity to model, with a minimal level of complexity, the advanced stage of the disease where no regeneration occurs, and fibrosis takes over. In fact, with the myriads of potential applications for in vitro 3D models, the need to customize their complexity according to the intended purpose [68] prompted us to tailor our system to perform muscle force evaluation retaining control and reproducibility, while being clinically relevant for personalized gene therapy screening.

As proof of the principle of the suitability of our system as a screening platform, we performed AAV-mediated microdystrophin gene transfer. Interestingly, optimal microdystrophin delivery in DMD MYOrganoids derived from different DMD iPSCs did not fully rescue DMD phenotype as it led to incomplete restoration of the components of the dystroglycan complex and partial attenuation of the inflammatory environment. Nonetheless, the improvement of muscle strength was significant in two of the three DMD iPSC-derived MYOrganoids. This phenomenon could be explained by the existence of compensatory mechanisms like adhesion complexes that act directly onto the structural maintenance of the fibers, as compared to the DAG complex that has a primary function mostly during development [69]**.** Remarkably the degree of rescue achieved differed among the cell lines used to derive DMD-MYOrganoids highlighting the importance of the genomic background in the response to treatments and the necessity for personalized medicine. Transcriptomic analysis unraveled the marginal effect of µDys gene transfer in correcting the DMD signature. Indeed, the persistence of dysregulated pathways not corrected by the gene transfer, could be related either to the lack of key

functional domains or the necessity to explore complementary strategies correcting additional parameters or to empower µDys efficacy to achieve full functional recovery.

Finally, our findings reveal a discrepancy to what was observed in animal model, where full rescue of muscle force and membrane stability is achieved [16,17]. This evidence supports the relevance of a human platform to unravel the potential limitations of the current treatments and consider genetic variations. Thus, pro-fibrotic DMD MYOrganoids might provide a valuable human *in vitro* counterpart to animal *in vivo* preclinical studies, for a more stringent evaluation of therapeutic efficiency based on muscle force parameters, with the potential to accelerate the identifications of new treatments as well as to unravel therapeutic limitations of current DMD treatments.

Acknowledgments

We express our gratitude to Rene Hummel (DMT), Guillaume Tanniou, and Nicolas Guerchet for their invaluable technical support in muscle force evaluation. We thank Guillaume Corre for the aid with RNA-seq analysis. We also extend our appreciation to Jérémie Cosette for the assistance in imaging and to the histology team for their technical expertise. Finally, we would like to thank Frederique Magdinier for generously providing the DMD iPSC dEx45 and Ctr1 iPSC.

Funding

This study was financially supported by the Institut National de la Sante et de la Recherche Medicale (INSERM) and by the "Association Française contre les Myopathies" (AFM).

Author contributions

SA and LPa designed the experiments. LPa performed most of the experiments, including iPSC culture, organoid generation, imaging, and muscle force analysis. LPi performed force analysis, gene expression analysis and western blot experiments. AJ analyzed conditioned media biomarkers and performed secretome analysis. LPa, MM contributed to muscle force analysis. AVH analyzed RNA-seq data. RE and GB performed electron microscopy analysis. AB generated and provided the immortalized human fibroblasts. SA and LPa performed data analysis and figure preparation. SA conceived, supervised the project, and wrote the manuscript. All authors discussed the results. SA, LPa, DI and IR reviewed and edited the manuscript.

Declaration of interests

All other authors declare they have no competing interests.

RESOURCE AVAILABILITY

Lead contact

Further information and requests for resources and reagents should be directed to and will be fulfilled by the lead contact, Sonia Albini (salbini@genethon.fr).

Material availability

Ctr2, corrDMDdEx8-9, DMDdEx8-9 and DMDdEx8-43 hIPS cell lines used in this study are restricted due to MTAs (Ref: MTA 2022 GENETHON - AIM _DMD, MMTA202109-0107, 2021-0296_MTA_CECS). This study did not generate new unique reagents.

Data and code availability

The data supporting the findings of this study are available within the article and its supplemental information. The RNA sequencing datasets generated in this study can be found in the NCBI Bioproject database (https://www.ncbi.nlm.nih.gov/bioproject) using the access number PRJNA1044721.

Microscopy and functional data reported in this paper will be shared by the lead contact upon request.

Any additional information required to reanalyze the data reported in this paper is available from the lead contact upon request.

EXPERIMENTAL MODELS

Induced pluripotent stem cells (iPSCs)

Human iPSCs used in the study were as follows: Ctr1 (AG08C5) derived from healthy fibroblasts (AG08498, Coriell Institute), Ctr2 (M180, CECS), IPSC DMDdEx45 (Coriell, GM25313); DMDdEx8-43 (M202, CECS) DMDdEx8-9 and corrDMDdEx8-9 (CRISPR-mediated skipping of mutated exons dEx6-9, isogenic control) (provided by Doctor E. Olson). iPSCs were maintained using mTeSRplus medium (Stem Cell Technologies) and passaged using ReleSR (Stem Cell Technologies) on Matrigel coated wells (Corning). iPSC engineering and muscle differentiation were performed adapting a transgene-based method previously described (Caputo et al. 2020; Albini et al. 2013). Quality control was performed regularly with Oct-4 and Nanog expression profile and mycoplasma testing and cells were used within 30 passages. Additionally, antibiotic and antimycotic solution (Merk-Millipore) was regularly added to each cell culture media.

All iPSC lines are engineered for transgene-based myotubes differentiation. Briefly, cells were nucleofected (4D Nucleofector, Lonza) with two enhanced versions of piggyBAC (ePB) containing respectively MyoD and BAF60c genes under tetracycline responsive promoter (Caputo L et al 2020). Additionally, iPSCs were regularly selected for the presence of the two ePBs with Puromycin 10 µg/ml and Blasticidin 20 µg/ml (Sigma-Aldrich).

Human immortalized fibroblasts

Human immortalized fibroblasts from control (AB1191, AIM) and DMD patient (AB1024, AIM) were generated and obtained from Myobank-AFM of Myology Institute from skin biopsies. Control and DMD human immortalized fibroblasts, used in co-culture with hiPSC in 3D MYOrganoids, were maintained in culture in DMEM High Glucose Lglut supplemented with 20% fetal bovine serum (FBS) and passaged using TrypleE (Gibco).

Human primary fibroblasts

Human primary fibroblasts from control (3 lines: 5-8898, 11-1610, 11-1973) and from DMD patients (3 lines, 5-11618, 5-12608, 5-11613) were obtained from DNA bank of Genethon. Fibroblasts were maintained in DMEM high glucose (Gibco) supplemented with 20 ng/ml recombinant human fibroblast growth factor (h-FGF) (Peprotech) and 20% fetal bovine serum (Gibco). Primary fibroblasts were passaged using TrypleE (Gibco)

METHOD DETAILS

Generation of MYOrganoids

MYOrganoids from iPSCs were generated adapting the protocol described for engineered heart tissue (Tiburcy et al. 2020). First, iPSC were induced with doxycycline 200 ng/µl for 24 hours to induce the expression of MyoD and Baf60c. The day after, 1.25 x 10^6 iPSC-committed were resuspended in 77 µl of growth media (SKM02, AMSbiokit) supplemented with hES cell Recovery (Stemgent) and molded in hydrogel composed by 40 µl of Bovine Collagen solution 6mg/ml (Sigma-Aldrich), 17.8 µl of Matrigel Growth Factor reduced (GFR, Corning) 10% v/v 3), 40µl 2X DMEM (Gibco) 4) and 5.2 µl of NaOH 0.05 N). For the generation of MYOrganoids including fibroblasts, 1.25 x 10^5 (ratio 1:10) fibroblasts were included in the iPSC-committed mix during hydrogel preparation. 180µl of hydrogel was casted into 48-well plate TM5 MyrPlate (Myriamed), containing in each well a pair of flexible poles (static stretchers) that support the growth of the engineered tissue in a ring shape. After 1 hour of polymerization at 37°C, growth media (SKM02, AMSbiokit) was added for 24 hours. On day 2 of the 3D, growth media (SKM02, AMSbiokit) was replaced by differentiation media (SKM03plus, AMSbiokit) and changed every day until day 14.

Muscle force analysis

Functional analyses were carried out on day 14 after 3D casting. Contraction experiments were performed using the MyoDynamics Muscle Strip System 840 MD (Danish Myo Technology A/S) and CS4 stimulator (Danish Myo Technology A/S). All functional analysis were performed at 37°C, 5% CO_2 95% O_2, in Tyrode's solution supplemented with 25 mM $NaHCO_3$. Optimal muscle length was determined by gradually stretching the muscle until 1.0 mN of passive tension registered. Functional tests were performed under isometric and eccentric conditions. MYOrganoids were electrically stimulated with 250 pulses of 30V, 4 ms width at the 125 Hz of frequency for both isometric and eccentric contractions. For eccentric analysis, MYOrganoids were 1 mm stretched at the 6.5 mm/s speed during the muscular contraction. Data collection and analysis was done by PowerLab device and LabChart software (ADInstruments, New Zealand) respectively. Each artificial tissue was subjected to 1 isometric contraction, 10 eccentric contractions and 1 isometric contraction. Fatigue is represented as percentage drop force between the first and the last isometric contraction. Where indicated, force is indirectly normalized for the CSA (Cross Section Area) calculated as muscle force (mN) x Lo (mm) x density (mg/mm3)/weight (mg) and expressed as mN/mm2. Engineered muscle density is experimentally determined as 2.089 mg/mm3.

Immunofluorescence

MYOrganoids that did not undergo functional analysis, have been analyzed for immunehistofluorescence. Briefly, the artificial tissues are fixed if 4% methanol-free paraformaldehyde (PFA) overnight on day 14. For whole mount staining, fixed MYOrganoids were permeabilized, stained and cleared with the MACS clearing kit (Miltenyi) according to manufacturer's instructions. Whole mount-stained organoids are then imaged with confocal microscope (LEICA STED SP8) at 10X magnification.

For staining on transversal or longitudinal sections, fixed MYOrganoids are dehydrated with a gradient of sucrose (7.5%-30%) over-day and embedded in OCT matrix in plastic mold. After 24 hours, embedded MYOrganoids are processed with the cryostat (LEICA) with 14 µm thick sections. Slices were then dried and fixed again with 4% methanol-free PFA (Invitrogen). Fixed sections are then blocked with serum cocktail (5% Goat serum and 5% Fetal bovine serum), before being stained overnight at +4°C with primary antibody. After that, slices are washed three times in PBS and hybridized with AlexaFluor secondary antibody accordingly to the host species of the first antibody. Stained slides were then covered with Fluoromont + Dapi (SouthernBiotech) and glass slide 1.5H. For imaging, sections are scanned with AxioScan microscope and confocal Leica SP8. Antibodies used are listed in the resources table (**Table S2**).

For 2D staining, cells are grown on µ-Dish 35 mm (Ibidi) and then fixed in 4% methanol-free PFA for 7 minutes. For membrane and cytoplasmatic stainings, cells are permeabilized with 0.15% Triton X-100 for 10 minutes and then washed with PBS for 5 minutes. For nuclear staining, cells are permeabilized with 0.25% Triton X-100 for 15 minutes. Permeabilized cells are then blocked with serum cocktail (5% Goat serum and 5% Fetal bovine serum), before being stained overnight at +4°C with primary antibody. Cells are then washed three times with PBS for 5 minutes and then hybridized with AlexaFluor secondary antibody according to the host species of the first antibody. After three washing of 5 minutes in PBS, nuclei are stained for 10 minutes with Hoechst 33342 (Invitrogen) at the final dilution of 2 µg/ml. For imaging, sections are scanned confocal Leica SP8. Antibodies used are listed in table S2.

Electron Microscopy studies

Electron microscopy analysis was prospectively performed on MYOtissue specimens that were fixed with glutaraldehyde (2.5%, pH 7.4), post fixed with osmium tetroxide (2%), dehydrated in a graded series of ethanol ranging from 30% to absolute solution and embedded in resin (EMBed-812, Electron Microscopy Sciences, USA). 80 nm thick sections from at least four blocks from Ctr iPSC-derived MYOrganoids in presence or absence of Ctr fibroblasts were stained with uranyl acetate and lead citrate. The grids were observed using a “JEOL 1400 Flash” electron microscope (120 kV) and were photo documented using a Xarosa camera (Soft Imaging System, France). Images covering whole longitudinal sections were assessed and representative images were used.

Images analysis

Myotubes alignment

FIJI and CellPose were used for image analysis. Myotube alignment was determined by angle measurement and by myotube circularity from cross-section cuts of MYOrganoids. Angles between two myotubes were measured with the “angle tool” function in FIJI, by drawing two lines perpendicular to two adjacent myotubes membrane. Myotubes circularity was determined by custom FIJI script. Briefly, myotubes cross section area was first segmented by pre-trained Cellpose2 cyto2 model [70] and then converted into Regions of Interest (ROIs) by Labels_To_Rois.py plugin (Waisman et al. 2021) for subsequent quantification on FIJI (Ferret

diameters X and Y). After that, the ratio between Feret's diameter on axis X and axis Y was assessed. At least 4 frames for 3 biological replicates have been analyzed.

Maturation and fusion index

Maturation index was assessed counting nuclei contained in striated myotubes identified by sarcomeric alpha actinin SAA staining in FIJI software and normalized for the total number of nuclei contained in myotubes. Fusion index has been calculated counting myotubes myosin heavy chain (MyHC) positive containing 1, 2, 3 or more than 3 nuclei as a percentage of the total number of nuclei. At least 4 frames for 3 biological replicates have been analyzed.

Z-disk length analysis

Z-disk length has been assessed by drawing straight lines in FIJI and by measuring the length in at least 10 mature myotubes per condition.

Fibronectin and phospo-SMAD3 quantification

Fibronectin protein has been quantified as "IntDen" which is the product of Area and Mean Gray Value on FIJI software. Phospho-SMAD3 has been measured as a percentage of positive nuclei. At least 4 frames for 3 biological replicates have been analyzed.

Dystrophin, α-dystroglycan and β-dystroglycan quantification

MYOtissue cross sections were stained sarcomeric alpha-actinin (SAA) for myotubes cytosol labeling. The Cellpose2 cyto2 model 10 was fine-tuned on manually myofiber-labeled images based on SAA staining (hyperparameters: n_epochs=200, learning_rate=0.05, weight_decay=0.0001). The labeled dataset used in fine-tuning was prepared in such a way that the model can simultaneously segment myotubes and ignore low-quality staining areas. Fine-tuned models were then used to extract myotubes masks. Reconstruction of myotubes masks was done using the cellpose package (Stringer et al. 2021). Reconstructed masks were then converted into Regions of Interest (ROIs) for subsequent quantification (each ROI corresponds to an individual myofiber) using the Labels_To_Rois.py FIJI plugin [71]. The generated ROIs were used for subsequent quantification using FIJI macro. Positive ROIs for dystrophin / alpha-dystroglycan / beta-dystroglycan signal were counted and represented as a percentage of the total ROIs of one image.

Gene expression analysis

For gene expression analysis, RNA was isolated from MYOrganoids by RNeasy micro kit (QIAGEN) accordingly to manufacturer's instructions, controlled and quantified by Nanodrop. Around 0.5-1µg of RNA was retro-transcribed to cDNA thanks to the RevertAid H Minus First Strand cDNA Synthesis Kit (Invitrogen). Droplet digital PCR was performed to assess the expression of myogenic factors (MyoD, MYH2, MYH7, MCK, PAX7), of fibrotic markers (COL1A, FN1) and µDystrophin, thanks to the QX200™ ddPCR™ EvaGreen Supermix (Biorad). Gene expression results in copy/µl are represented as fold change to the expression of MyoD normalized for GAPDH housekeeping gene. Primers used are listed in table S3.

Biomarker analysis from conditioned media

Media was collected just before muscle functional analysis after being in culture for 24 hours (media "before"). After the exercise, MYOrganoids were kept in culture with fresh media for additional 24 hours (media "after"). The media was then analyzed for assessment of cytokines concentration. Secretome analysis was performed using the MILLIPLEX® Multiplex Assays Using Luminex® Technology (Millipore), according to manufacturer's instructions. Briefly, media was analyzed for determining the concentration of tumor necrosis factor-alpha (TNFα), interleukin 6 (IL6) and interleukin 8 (IL8).

AAV production and MYOrganoids infection

Recombinant AAVs were produced as previously described (Bourg et al. 2022) using AAV9 serotype. Purification was performed using affinity chromatography and titration was done by ddPCR using transgene-specific primers. For optimization of infection, an AAV9-CMV-GFP construct was used. The micro-dystrophin transgene used in the study, under the control of spc512 promoter, was an optimized version of the construct used for GENETHON's preclinical investigation and clinical trial (Le Guiner et al. 2017b), with deletion from spectrin-like repeats 4 to 23 and full C-terminal truncation, here referred as µDys. Infection in MYOrganoids was performed by delivering the AAV9 particles diluted into the differentiation media at day 7, at two different doses: 1^9 vg/MYOtissue (low dose) and 5^10 vg/MYOtissue (high dose). Media was replaced after 24 hours from the infection and changed daily until day 14.

Viral copy number analysis

Viral DNA was extracted from mature MYOrganoids by NucleoMag Pathogen kit (Macherey Nagel) using Kingfisher instrument (Thermofisher). DNA yield and purity was assessed by Nanodrop; VCN (viral copy number) was identified by droplet digital PCR using supermix for probe (Biorad). Results are shown as copy number variation using P0 as reference DNA. Primers used are listed in Table S3.

Capillary western blot analysis

MYOrganoids proteins were extracted in RIPA buffer supplemented with Protease Inhibitor Cocktail EDTA-free (Roche) and Benzonase by homogenization. Total proteins were then quantified by BCA method, thanks to the Pierce 660 protein assay kit (Invitrogen) according to manufacturer's instructions. Protein detection has been performed by capillary western blot, thanks to the JESS protein simple (Bio-techne), according to manufacturer's directions. Dystrophin detection (both full-length and µDystrophin) has been performed by the antibody DysB (NCL-DYSB, Leica, 1:20) and its expression has been quantified by total protein normalization.

RNA sequencing and transcriptomic analysis

The RNA quality of samples was verified using the Bioanalyzer 2100 (Agilent) and Qubit fluorometric quantification (ThermoFisher Scientific). The samples that had an RNA integrity number higher than 9 were used for RNA sequencing (Genewiz). The Stranded Total RNA Library Prep Kit (Illumina) was used to create the sequencing libraries, which were sequenced following the Illumina protocol on the NovaSeq instrument (Illumina), resulting in approximately 20 million paired-end reads per library. The paired-end reads were filtered and

subjected to quality control using fastp (Chen et al. 2018). They were then mapped to the GRCh38/hg38 genome using HISAT2 [72] count tables were generated using htseq-count [73]. Differentially expressed genes (DEGs) were identified using the DESeq2 R package with p value adjusted by Benjamin-Hochberg procedure less than 0.05. Pathway analysis was carried out in R-Studio (version 4.0.3) using functional class scoring with Gene Set Enrichment Analysis [74,75].

Statistical analysis

All data were analyzed by GraphPad Prism 9.5.1 software. Parametric tests such as t-tests and ANOVA were used for statistical comparison. To compare two groups, initially F-test was used to compare variances. If there was no difference in variances, statistical comparison was performed using unpaired t-test. To compare multiple groups, we used one-way ANOVA with Tukey's correction for multiple comparison tests**.** Results were considered significantly different at $p < 0.05$. Graphs were generated using Graphpad Prism v9 or R version 3.6.2, The figures display the mean ± standard error of the mean.

References

1. Mendell, J. R. *et al.* Evidence-based path to newborn screening for Duchenne muscular dystrophy. *Annals of neurology* **71**, 304–313 (2012).
2. Hoffman, E. P., Brown, R. H. & Kunkel, L. M. Dystrophin: the protein product of the Duchenne muscular dystrophy locus. *Cell* **51**, 919–928 (1987).
3. Ervasti, J. M. & Campbell, K. P. A role for the dystrophin-glycoprotein complex as a transmembrane linker between laminin and actin. *The Journal of cell biology* **122**, 809–823 (1993).
4. Petrof, B. J., Shrager, J. B., Stedman, H. H., Kelly, A. M. & Sweeney, H. L. Dystrophin protects the sarcolemma from stresses developed during muscle contraction. *Proceedings of the National Academy of Sciences of the United States of America* **90**, 3710–3714 (1993).
5. Hoffman, E. P., Brown, R. H. & Kunkel, L. M. Dystrophin: the protein product of the Duchenne muscular dystrophy locus. *Cell* **51**, 919–928 (1987).
6. Hoffman, E. P. The discovery of dystrophin, the protein product of the Duchenne muscular dystrophy gene. *FEBS Journal* **287**, 3879–3887 (2020).
7. Davies, K. E. & Nowak, K. J. Molecular mechanisms of muscular dystrophies: old and new players. *Nature reviews. Molecular cell biology* **7**, 762–773 (2006).
8. Ennen, J. P., Verma, M. & Asakura, A. Vascular-targeted therapies for Duchenne muscular dystrophy. *Skeletal muscle* **3**, (2013).
9. Porter, J. D. *et al.* A chronic inflammatory response dominates the skeletal muscle molecular signature in dystrophin-deficient mdx mice. *Human molecular genetics* **11**, 263–272 (2002).
10. Amor, F. *et al.* Cholesterol metabolism is a potential therapeutic target in Duchenne muscular dystrophy. *Journal of cachexia, sarcopenia and muscle* **12**, 677–693 (2021).
11. Caputo, L. *et al.* Acute conversion of patient-derived Duchenne muscular dystrophy iPSC into myotubes reveals constitutive and inducible over-activation of TGFβ-dependent pro-fibrotic signaling. *Skeletal Muscle* **10**, (2020).
12. Wynn, T. A. Cellular and molecular mechanisms of fibrosis. *Journal of Pathology* **214**, 199–210 (2008).
13. Kharraz, Y., Guerra, J., Pessina, P., Serrano, A. L. & Muñoz-Cánoves, P. Understanding the process of fibrosis in Duchenne muscular dystrophy. *BioMed research international* **2014**, 965631 (2014).
14. Mendell, J. R. *et al.* duan. *Molecular therapy : the journal of the American Society of Gene Therapy* **29**, 464–488 (2021).
15. Aguti, S., Malerba, A. & Zhou, H. The progress of AAV-mediated gene therapy in neuromuscular disorders. *Expert opinion on biological therapy* **18**, 681–693 (2018).
16. Duan, D. Systemic AAV Micro-dystrophin Gene Therapy for Duchenne Muscular Dystrophy. *Molecular Therapy* **26**, 2337–2356 (2018).
17. Le Guiner, C. *et al.* Long-term microdystrophin gene therapy is effective in a canine model of Duchenne muscular dystrophy. *Nature Communications* **8**, (2017).

18. Elangkovan, N. & Dickson, G. Gene Therapy for Duchenne Muscular Dystrophy. *Journal of neuromuscular diseases* **8**, S303–S316 (2021).
19. Harper, S. Q. *et al.* Modular flexibility of dystrophin: implications for gene therapy of Duchenne muscular dystrophy. *Nature medicine* **8**, 253–261 (2002).
20. Wang, B., Li, J. & Xiao, X. Adeno-associated virus vector carrying human minidystrophin genes effectively ameliorates muscular dystrophy in mdx mouse model. *Proceedings of the National Academy of Sciences of the United States of America* **97**, 13714–13719 (2000).
21. Fabb, S. A., Wells, D. J., Serpente, P. & Dickson, G. Adeno-associated virus vector gene transfer and sarcolemmal expression of a 144 kDa micro-dystrophin effectively restores the dystrophin-associated protein complex and inhibits myofibre degeneration in nude/mdx mice. *Human molecular genetics* **11**, 733–741 (2002).
22. Duan, D. Duchenne Muscular Dystrophy Gene Therapy in 2023: Status, Perspective, and Beyond. *Human gene therapy* **34**, 345–349 (2023).
23. Elangkovan, N. & Dickson, G. Gene Therapy for Duchenne Muscular Dystrophy. *Journal of neuromuscular diseases* **8**, S303–S316 (2021).
24. Takahashi, K. *et al.* Induction of Pluripotent Stem Cells from Adult Human Fibroblasts by Defined Factors. *Cell* **131**, 861–872 (2007).
25. Tornabene, P. *et al.* Intein-mediated protein trans-splicing expands adeno-associated virus transfer capacity in the retina. *Science translational medicine* **11**, (2019).
26. Clevers, H. Modeling Development and Disease with Organoids. *Cell* **165**, 1586–1597 (2016).
27. Hofer, M. & Lutolf, M. P. Engineering organoids. *Nature reviews. Materials* **6**, 402–420 (2021).
28. Shin, M. K. *et al.* Generation of Skeletal Muscle Organoids from Human Pluripotent Stem Cells to Model Myogenesis and Muscle Regeneration. *International Journal of Molecular Sciences* **23**, (2022).
29. Pinton, L. *et al.* 3D human induced pluripotent stem cell-derived bioengineered skeletal muscles for tissue, disease and therapy modeling. *Nature protocols* **18**, (2023).
30. Rao, L., Qian, Y., Khodabukus, A., Ribar, T. & Bursac, N. Engineering human pluripotent stem cells into a functional skeletal muscle tissue. *Nature communications* **9**, (2018).
31. Shahriyari, M. *et al.* Engineered skeletal muscle recapitulates human muscle development, regeneration and dystrophy. *Journal of Cachexia, Sarcopenia and Muscle* **13**, 3106–3121 (2022).
32. Garita-Hernandez, M. *et al.* AAV-Mediated Gene Delivery to 3D Retinal Organoids Derived from Human Induced Pluripotent Stem Cells. *International journal of molecular sciences* **21**, (2020).
33. Kruczek, K. *et al.* Gene Therapy of Dominant CRX-Leber Congenital Amaurosis using Patient Stem Cell-Derived Retinal Organoids. *Stem cell reports* **16**, 252–263 (2021).
34. Khabou, H. *et al.* Noninvasive gene delivery to foveal cones for vision restoration. *JCI insight* **3**, (2018).
35. Caputo, L. *et al.* Acute conversion of patient-derived Duchenne muscular dystrophy iPSC into myotubes reveals constitutive and inducible over-activation of TGFβ-dependent pro-fibrotic signaling. *Skeletal Muscle* **10**, (2020).
36. Albini, S. *et al.* Epigenetic Reprogramming of Human Embryonic Stem Cells into Skeletal Muscle Cells and Generation of Contractile Myospheres. *Cell Reports* **3**, 661–670 (2013).
37. Albini, S. & Puri, P. L. Generation of Myospheres From hESCs by Epigenetic Reprogramming. *Journal of Visualized Experiments* (2014) doi:10.3791/51243.
38. Pinton, L. *et al.* 3D human induced pluripotent stem cell-derived bioengineered skeletal muscles for tissue, disease and therapy modeling. *Nature protocols* (2023) doi:10.1038/S41596-022-00790-8.
39. Tiburcy, M., Meyer, T., Soong, P. L. & Zimmermann, W. H. Collagen-based engineered heart muscle. *Methods in molecular biology (Clifton, N.J.)* **1181**, 167–176 (2014).
40. Rao, N. *et al.* Fibroblasts influence muscle progenitor differentiation and alignment in contact independent and dependent manners in organized co-culture devices. *Biomedical microdevices* **15**, 161 (2013).
41. Mathew, S. J. *et al.* Connective tissue fibroblasts and Tcf4 regulate myogenesis. *Development (Cambridge, England)* **138**, 371–384 (2011).
42. Bersini, S. *et al.* Engineering an Environment for the Study of Fibrosis: A 3D Human Muscle Model with Endothelium Specificity and Endomysium. *Cell reports* **25**, 3858-3868.e4 (2018).
43. Saleh, K. K. *et al.* Single cell sequencing maps skeletal muscle cellular diversity as disease severity increases in dystrophic mouse models. *iScience* **25**, (2022).
44. Giordani, L. *et al.* High-Dimensional Single-Cell Cartography Reveals Novel Skeletal Muscle-Resident Cell Populations. *Molecular cell* **74**, 609-621.e6 (2019).
45. Petrany, M. J. *et al.* Single-nucleus RNA-seq identifies transcriptional heterogeneity in multinucleated skeletal myofibers. *Nature communications* **11**, (2020).
46. Karlsen, A. *et al.* Distinct myofibre domains of the human myotendinous junction revealed by single-nucleus RNA sequencing. *Journal of cell science* **136**, (2023).

47. Thorsteinsdottir, S., Deries, M., Cachaço, A. S. & Bajanca, F. The extracellular matrix dimension of skeletal muscle development. *Developmental Biology* **354**, 191–207 (2011).
48. Costantini, M. *et al.* Biofabricating murine and human myo-substitutes for rapid volumetric muscle loss restoration. *EMBO molecular medicine* **13**, (2021).
49. Al Tanoury, Z. *et al.* Prednisolone rescues Duchenne muscular dystrophy phenotypes in human pluripotent stem cell-derived skeletal muscle in vitro. *Proceedings of the National Academy of Sciences of the United States of America* **118**, (2021).
50. Minato, K. *et al.* Measurement of Lateral Transmission of Force in the Extensor Digitorum Longus Muscle of Young and Old Mice. *International Journal of Molecular Sciences* **22**, (2021).
51. Erdogan, B. R. *et al.* Normalization of organ bath contraction data for tissue specimen size: does one approach fit all? *Naunyn-Schmiedeberg's archives of pharmacology* **393**, 243–251 (2020).
52. Santos, G. L. *et al.* Fibroblast Derived Human Engineered Connective Tissue for Screening Applications. *Journal of visualized experiments : JoVE* **2021**, (2021).
53. Li, M., Dickinson, C. E., Finkelstein, E. B., Neville, C. M. & Sundback, C. A. The role of fibroblasts in self-assembled skeletal muscle. *Tissue engineering. Part A* **17**, 2641–2650 (2011).
54. Kühl, U. *et al.* Role of muscle fibroblasts in the deposition of type-IV collagen in the basal lamina of myotubes. *Differentiation; research in biological diversity* **28**, 164–172 (1984).
55. Mann, C. J. *et al.* Aberrant repair and fibrosis development in skeletal muscle. *Skeletal Muscle* **1**, 21 (2011).
56. Kyrychenko, V. *et al.* Functional correction of dystrophin actin binding domain mutations by genome editing. *JCI insight* **2**, (2017).
57. Childers, M. K. *et al.* Eccentric contraction injury in dystrophic canine muscle. *Archives of physical medicine and rehabilitation* **83**, 1572–1578 (2002).
58. Elangkovan, N. & Dickson, G. Gene Therapy for Duchenne Muscular Dystrophy. *Journal of Neuromuscular Diseases* **8**, S303 (2021).
59. Manini, A., Abati, E., Nuredini, A., Corti, S. & Comi, G. Pietro. Adeno-Associated Virus (AAV)-Mediated Gene Therapy for Duchenne Muscular Dystrophy: The Issue of Transgene Persistence. *Frontiers in Neurology* **12**, 814174 (2021).
60. Aguti, S., Malerba, A. & Zhou, H. The progress of AAV-mediated gene therapy in neuromuscular disorders. *Expert opinion on biological therapy* **18**, 681–693 (2018).
61. Elangkovan, N. & Dickson, G. Gene Therapy for Duchenne Muscular Dystrophy. *Journal of Neuromuscular Diseases* **8**, S303 (2021).
62. Lapidos, K. A., Kakkar, R. & McNally, E. M. The dystrophin glycoprotein complex: signaling strength and integrity for the sarcolemma. *Circulation research* **94**, 1023–1031 (2004).
63. Rosenberg, A. S. *et al.* Immune-mediated pathology in Duchenne muscular dystrophy. *Science Translational Medicine* **7**, 299rv4-299rv4 (2015).
64. Madden, L., Juhas, M., Kraus, W. E., Truskey, G. A. & Bursac, N. Bioengineered human myobundles mimic clinical responses of skeletal muscle to drugs. *eLife* **4**, (2015).
65. Khodabukus, A. *et al.* Electrical stimulation increases hypertrophy and metabolic flux in tissue-engineered human skeletal muscle. *Biomaterials* (2018) doi:10.1016/j.biomaterials.2018.08.058.
66. Barton, E. R. *et al.* Measuring isometric force of isolated mouse muscles in vitro. (2008).
67. Chal, J. *et al.* Differentiation of pluripotent stem cells to muscle fiber to model Duchenne muscular dystrophy. *Nature biotechnology* **33**, 962–9 (2015).
68. Bersini, S., Arrigoni, C., Talò, G., Candrian, C. & Moretti, M. Complex or not too complex? One size does not fit all in next generation microphysiological systems. *iScience* **27**, (2024).
69. Mirouse, V. Evolution and developmental functions of the dystrophin-associated protein complex: beyond the idea of a muscle-specific cell adhesion complex. *Front Cell Dev Biol* **11**, (2023).
70. Stringer, C., Wang, T., Michaelos, M. & Pachitariu, M. Cellpose: a generalist algorithm for cellular segmentation. *Nature methods* **18**, 100–106 (2021).
71. Waisman, A., Norris, A. M., Elías Costa, M. & Kopinke, D. Automatic and unbiased segmentation and quantification of myofibers in skeletal muscle. *Scientific reports* **11**, (2021).
72. Kim, D., Langmead, B. & Salzberg, S. L. HISAT: a fast spliced aligner with low memory requirements. *Nature methods* **12**, 357–360 (2015).
73. Love, M. I., Huber, W. & Anders, S. Moderated estimation of fold change and dispersion for RNA-seq data with DESeq2. *Genome biology* **15**, (2014).
74. Subramanian, A. *et al.* Gene set enrichment analysis: a knowledge-based approach for interpreting genome-wide expression profiles. *Proceedings of the National Academy of Sciences of the United States of America* **102**, 15545–15550 (2005).
75. Mootha, V. K. *et al.* PGC-1alpha-responsive genes involved in oxidative phosphorylation are coordinately downregulated in human diabetes. *Nature genetics* **34**, 267–273 (2003).

Figure 1

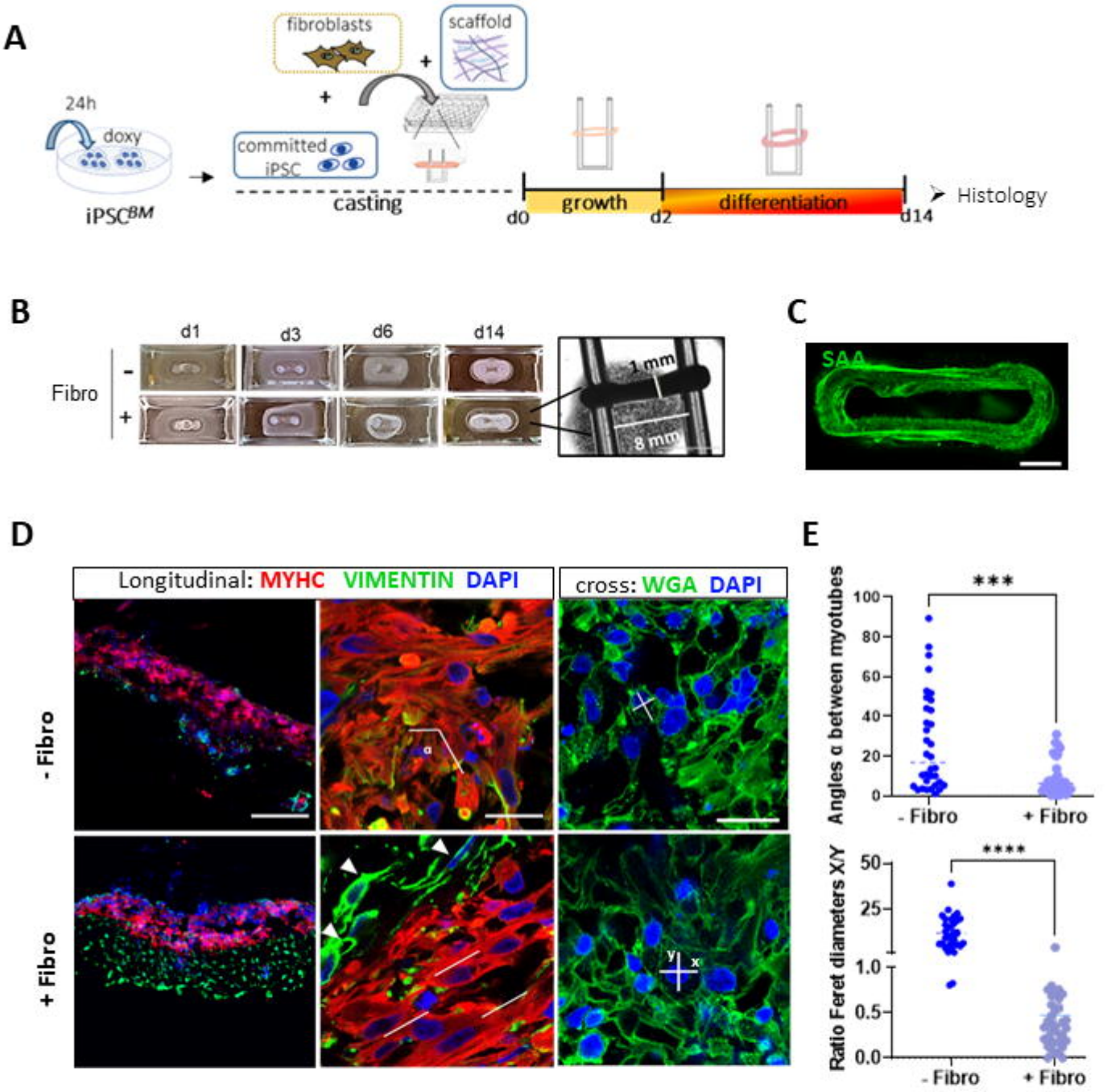
A
fibroblasts
scaffold
24h
doxy
iPSC^BM
committed iPSC
casting
growth
differentiation
d0
d2
d14
Histology
B
d1
d3
d6
d14
Fibro
-
+
1 mm
8 mm
C
SAA
D
Longitudinal: MYHC VIMENTIN DAPI
cross: WGA DAPI
- Fibro
+ Fibro
α
y
x
E
Angles α between myotubes
***
- Fibro
+ Fibro
Ratio Feret diameters X/Y
****

Figure 2

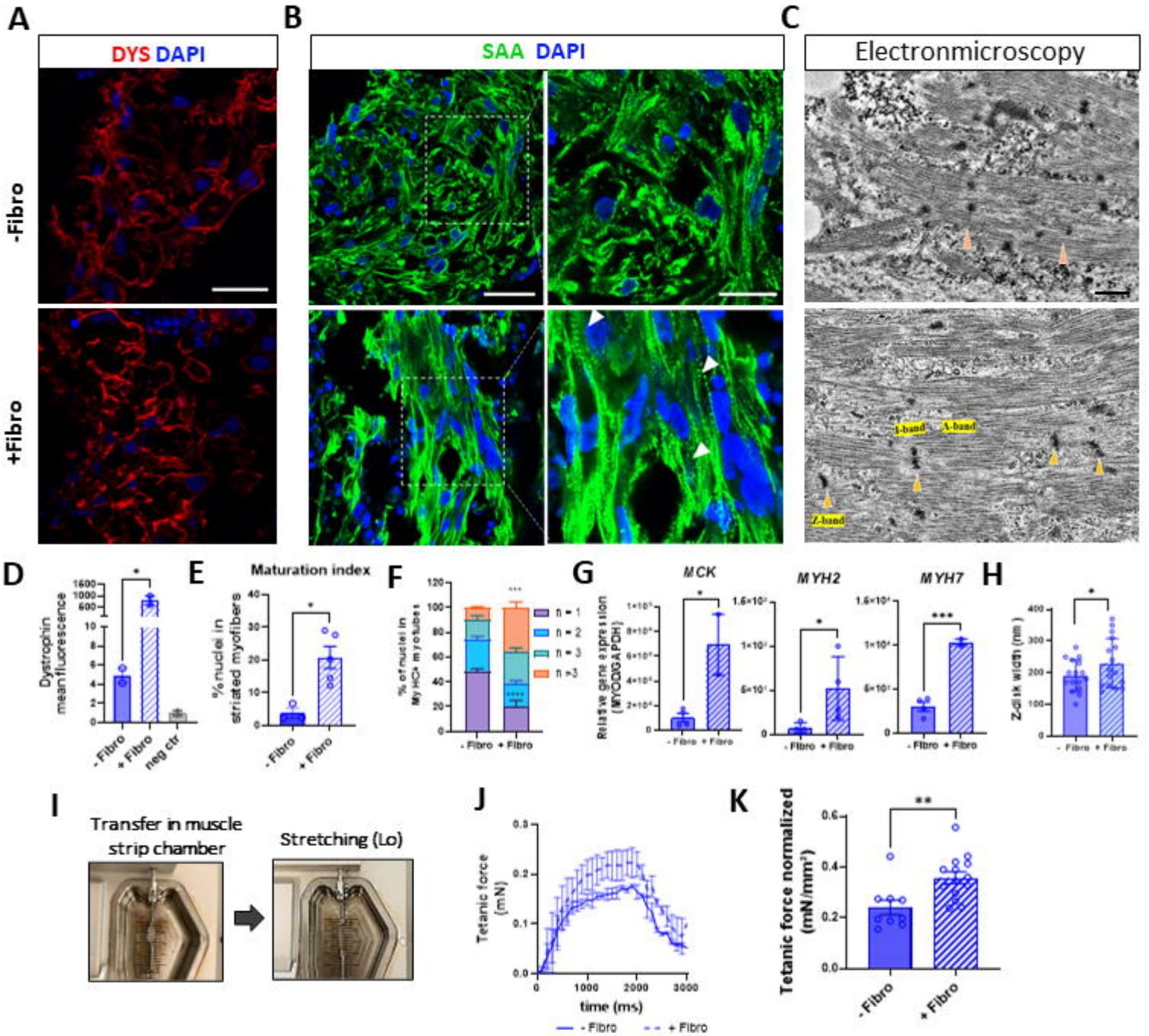
A
DYS DAPI
-Fibro
+Fibro
B
SAA DAPI
C
Electronmicroscopy
I-band
A-band
Z-band
D
Dystrophin mean fluorescence
- Fibro
+ Fibro
neg ctr
E
Maturation index
% nuclei in striated myofibers
F
% of nuclei in MyHC+ myotubes
n = 1
n = 2
n = 3
n >3
G
MCK
MYH2
MYH7
Relative gene expression (MYOD/GAPDH)
H
Z-disk width (nm)
I
Transfer in muscle strip chamber
Stretching (Lo)
J
Tetanic force (mN)
time (ms)
K
Tetanic force normalized (mN/mm²)

Figure 3

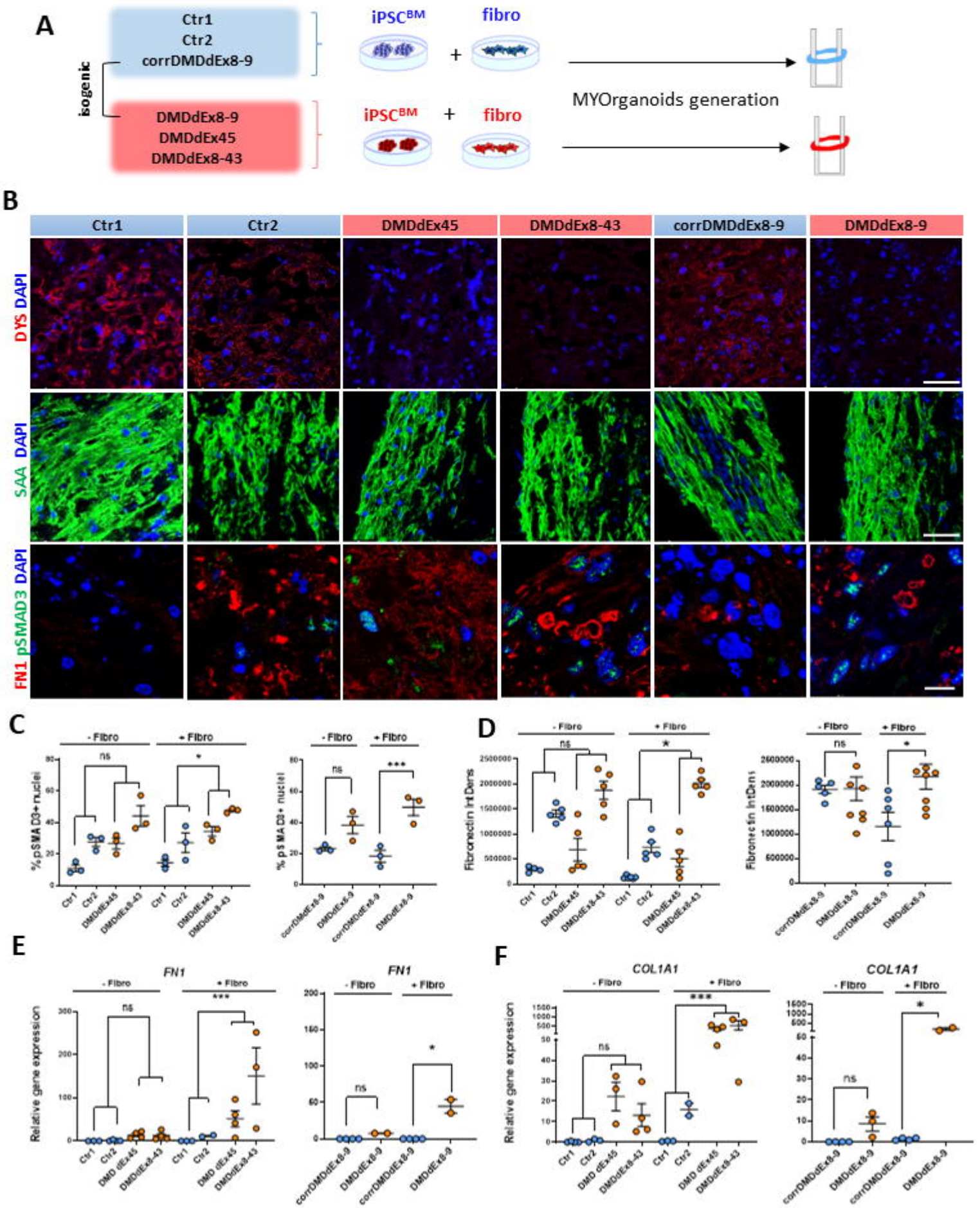
A
isogenic
Ctr1
Ctr2
corrDMDdEx8-9
DMDdEx8-9
DMDdEx45
DMDdEx8-43
iPSC^BM
fibro
MYOrganoids generation
B
Ctr1
Ctr2
DMDdEx45
DMDdEx8-43
corrDMDdEx8-9
DMDdEx8-9
DYS DAPI
SAA DAPI
FN1 pSMAD3 DAPI
C
- Fibro
+ Fibro
% pSMAD3+ nuclei
D
Fibronectin IntDens
E
FN1
Relative gene expression
F
COL1A1
Relative gene expression

Figure 4

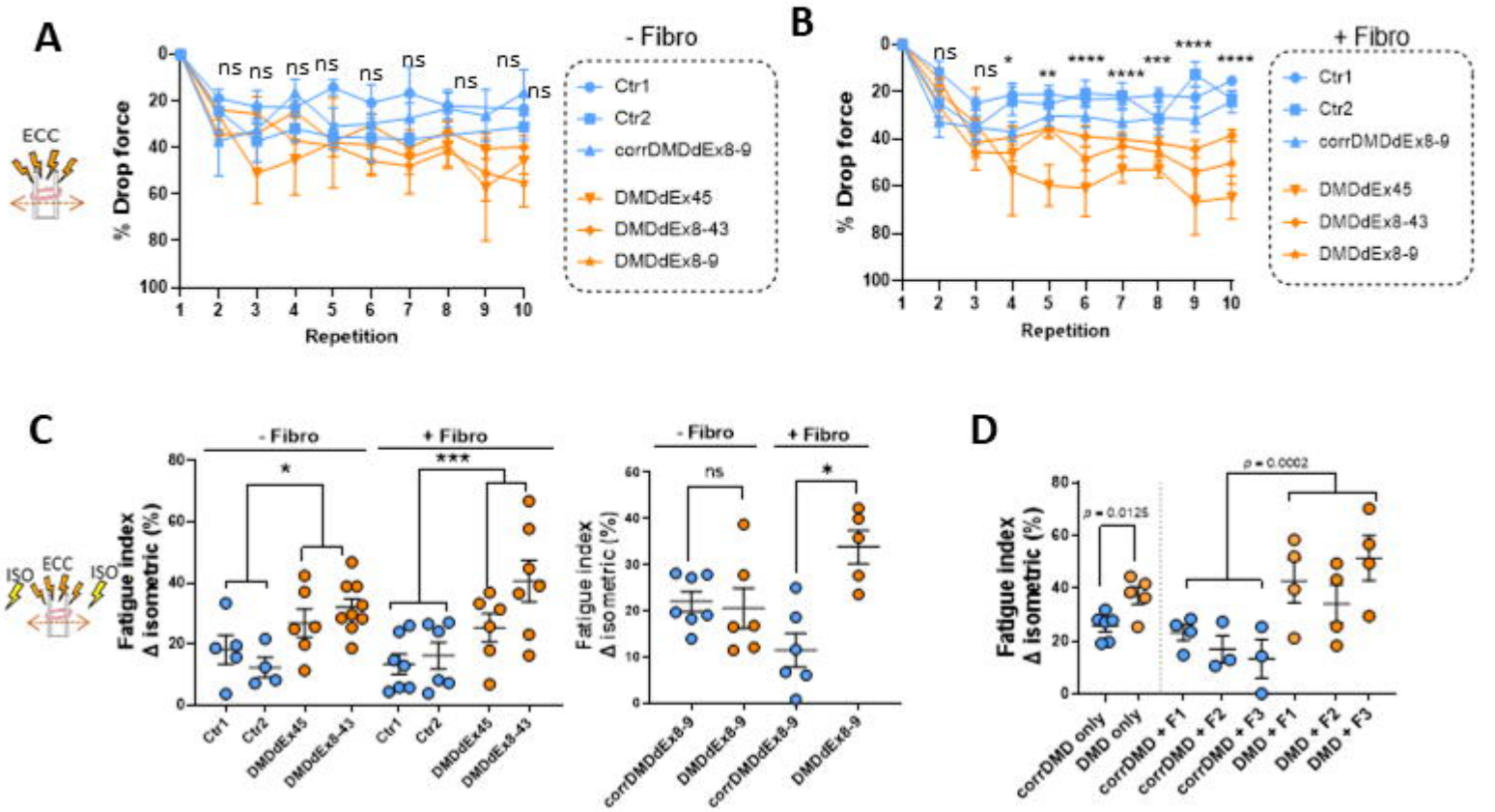
A
ECC
% Drop force
Repetition
- Fibro
Ctr1
Ctr2
corrDMDdEx8-9
DMDdEx45
DMDdEx8-43
DMDdEx8-9
B
+ Fibro
C
ISO
ECC
ISO
Fatigue index
Δ isometric (%)
- Fibro
+ Fibro
D
p = 0.0125
p = 0.0002
corrDMD only
DMD only
corrDMD + F1
corrDMD + F2
corrDMD + F3
DMD + F1
DMD + F2
DMD + F3

Figure 5

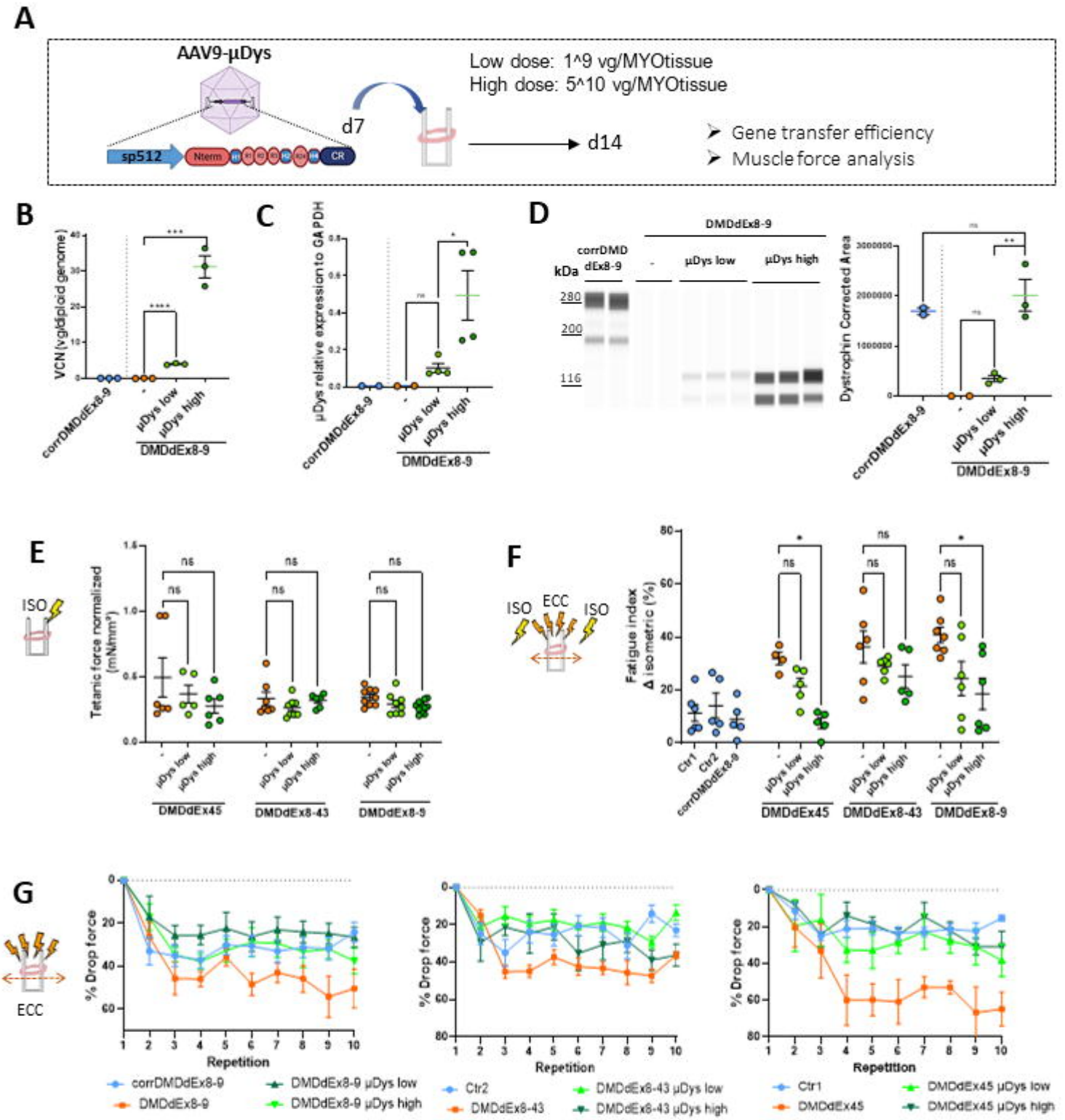
A
AAV9-µDys
sp512
Nterm
CR
d7
d14
Low dose: 1^9 vg/MYOtissue
High dose: 5^10 vg/MYOtissue
Gene transfer efficiency
Muscle force analysis
B
VCN (vg/diploid genome)
corrDMDdEx8-9
µDys low
µDys high
DMDdEx8-9
C
µDys relative expression to GAPDH
D
DMDdEx8-9
corrDMD dEx8-9
kDa
280
200
116
µDys low
µDys high
Dystrophin Corrected Area
E
ISO
Tetanic force normalized (mN/mm²)
DMDdEx45
DMDdEx8-43
DMDdEx8-9
F
ISO
ECC
ISO
Fatigue index Δ isometric (%)
Ctr1
Ctr2
G
ECC
% Drop force
Repetition
corrDMDdEx8-9
DMDdEx8-9
DMDdEx8-9 µDys low
DMDdEx8-9 µDys high
Ctr2
DMDdEx8-43
DMDdEx8-43 µDys low
DMDdEx8-43 µDys high
Ctr1
DMDdEx45
DMDdEx45 µDys low
DMDdEx45 µDys high

Figure 6

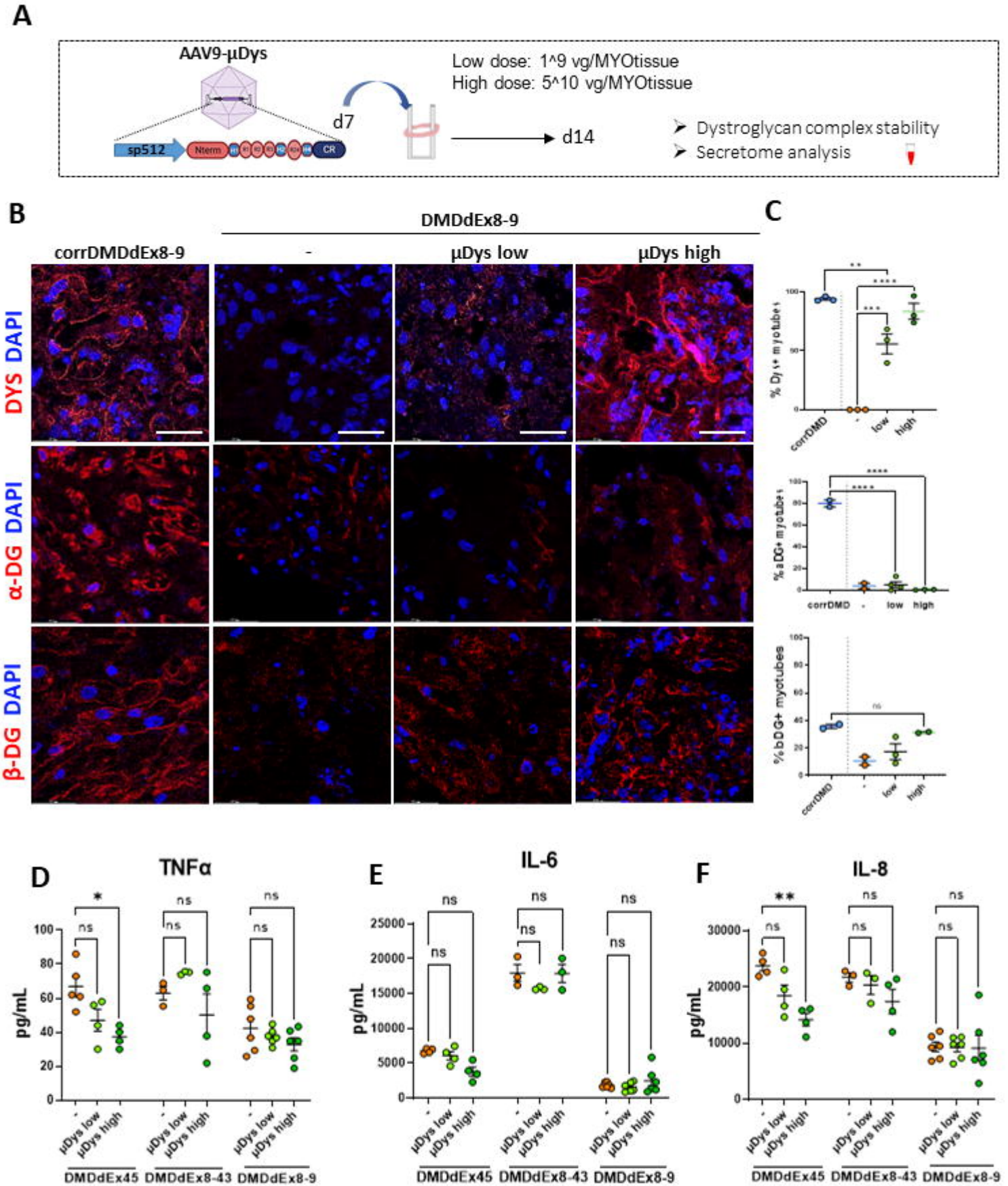
A
AAV9-µDys
sp512
Nterm
CR
d7
d14
Low dose: 1^9 vg/MYOtissue
High dose: 5^10 vg/MYOtissue
Dystroglycan complex stability
Secretome analysis
B
DMDdEx8-9
corrDMDdEx8-9
-
µDys low
µDys high
DYS DAPI
α-DG DAPI
β-DG DAPI
C
% Dys+ myotubes
% aDG+ myotubes
% bDG+ myotubes
corrDMD
low
high
D
TNFα
pg/mL
E
IL-6
F
IL-8
DMDdEx45
DMDdEx8-43
DMDdEx8-9
ns

Figure 7

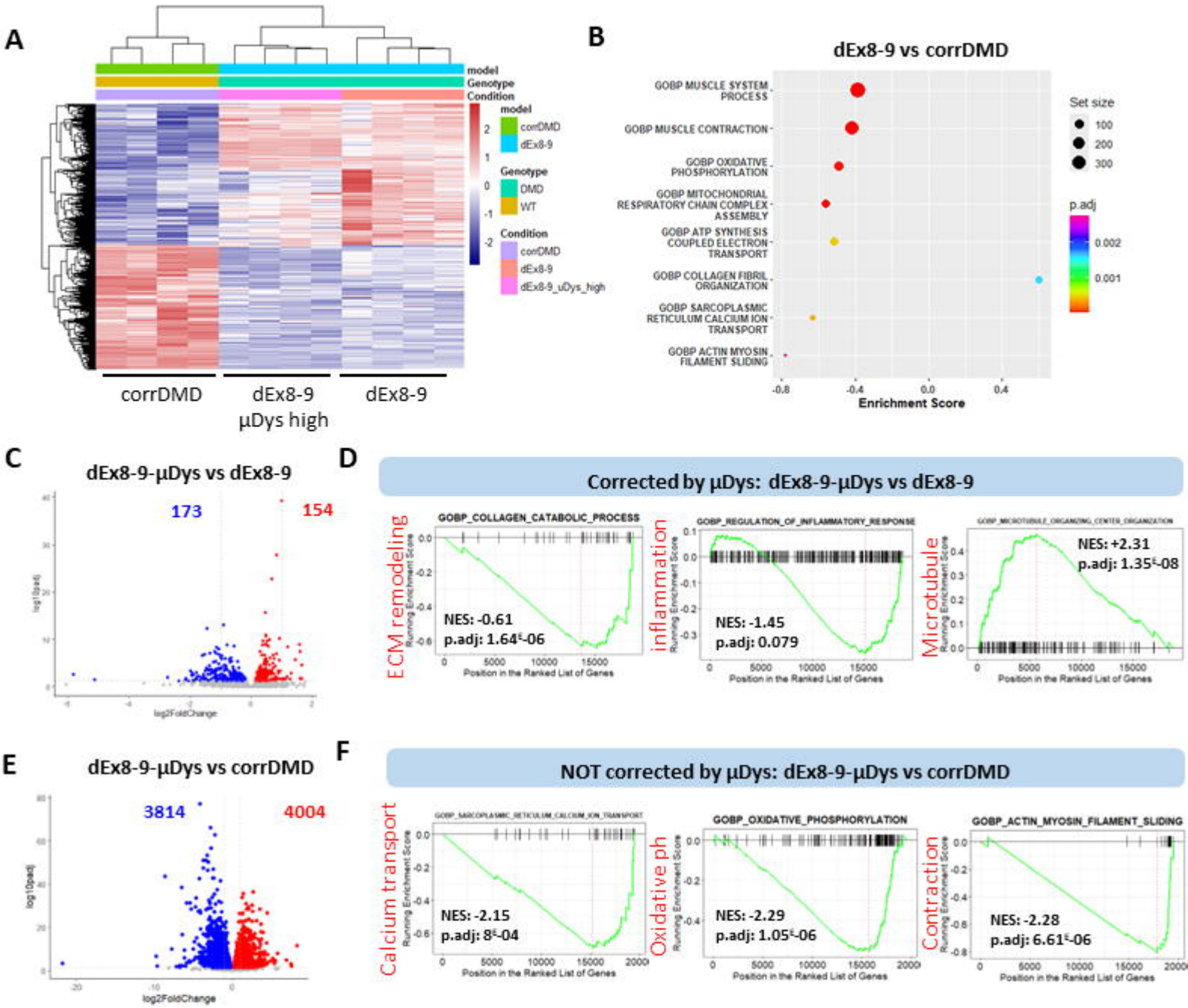
A
model
Genotype
Condition
model
corrDMD
dEx8-9
Genotype
DMD
WT
Condition
corrDMD
dEx8-9
dEx8-9_uDys_high
corrDMD
dEx8-9
dEx8-9
µDys high
B
dEx8-9 vs corrDMD
GOBP MUSCLE SYSTEM PROCESS
GOBP MUSCLE CONTRACTION
GOBP OXIDATIVE PHOSPHORYLATION
GOBP MITOCHONDRIAL RESPIRATORY CHAIN COMPLEX ASSEMBLY
GOBP ATP SYNTHESIS COUPLED ELECTRON TRANSPORT
GOBP COLLAGEN FIBRIL ORGANIZATION
GOBP SARCOPLASMIC RETICULUM CALCIUM ION TRANSPORT
GOBP ACTIN MYOSIN FILAMENT SLIDING
Enrichment Score
Set size
100
200
300
p.adj
0.002
0.001
C
dEx8-9-µDys vs dEx8-9
173
154
log2FoldChange
D
Corrected by µDys: dEx8-9-µDys vs dEx8-9
ECM remodeling
GOBP_COLLAGEN_CATABOLIC_PROCESS
NES: -0.61
p.adj: 1.64E-06
inflammation
GOBP_REGULATION_OF_INFLAMMATORY_RESPONSE
NES: -1.45
p.adj: 0.079
Microtubule
NES: +2.31
p.adj: 1.35E-08
Position in the Ranked List of Genes
E
dEx8-9-µDys vs corrDMD
3814
4004
log2FoldChange
F
NOT corrected by µDys: dEx8-9-µDys vs corrDMD
Calcium transport
NES: -2.15
p.adj: 8E-04
Oxidative ph
GOBP_OXIDATIVE_PHOSPHORYLATION
NES: -2.29
p.adj: 1.05E-06
Contraction
GOBP_ACTIN_MYOSIN_FILAMENT_SLIDING
NES: -2.28
p.adj: 6.61E-06
Position in the Ranked List of Genes